Nanoscale

FEATURE ARTICLE

View Article Online
View Journal | View Issue

Cite this: *Nanoscale*, 2015, **7**, 1566

Nanostructuring graphene for controlled and reproducible functionalization

Kunal S. Mali,* John Greenwood, Jinne Adisoejoso, Roald Phillipson and Steven De Feyter*

Received 3rd November 2014,
Accepted 10th December 2014

DOI: 10.1039/c4nr06470d

www.rsc.org/nanoscale

The 'graphene rush' that started almost a decade ago is far from over. The dazzling properties of graphene have long warranted a number of applications in various domains of science and technology. Harnessing the exceptional properties of graphene for practical applications however has proved to be a massive task. Apart from the challenges associated with the large-scale production of the material, the intrinsic zero band gap, the inherently low reactivity and solubility of pristine graphene preclude its use in several high- as well as low-end applications. One of the potential solutions to these problems is the surface functionalization of graphene using organic building blocks. The 'surface-only' nature of graphene allows the manipulation of its properties not only by covalent chemical modification but also *via* non-covalent interactions with organic molecules. Significant amount of research efforts have been directed towards the development of functionalization protocols for modifying the structural, electronic, and chemical properties of graphene. This feature article provides a glimpse of recent progress in the molecular functionalization of surface supported graphene using non-covalent as well as covalent chemistry.

I. Introduction

Graphene is a single atom thick sheet of sp^2-hybridized carbon bonded in a honeycomb lattice.[1] After its first successful isolation in the form of freestanding monolayer films in 2004 together with the revelation of its unusual physics,[2] graphene has garnered tremendous scientific interest from both fundamental as well as applied point of view. This is mainly due to its unique electronic, optical, mechanical and thermal properties, which outperform most of the existing materials.[3,4] Graphene shows a remarkably high electron mobility of 2.0×10^5 cm^2 V^{-1} s^{-1} at room temperature.[5] Furthermore, the symmetry of the conductance measurements indicates identical hole mobility. With a Young's modulus of 1 TPa and an intrinsic strength of 130 GPa, it is the strongest material ever known.[6] At the same time it is flexible and can be stretched up

KU Leuven-University of Leuven, Department of Chemistry, Division of Molecular Imaging and Photonics Celestijnenlaan 200F, B-3001 Leuven, Belgium.
E-mail: Kunal.Mali@chem.kuleuven.be, Steven.DeFeyter@chem.kuleuven.be

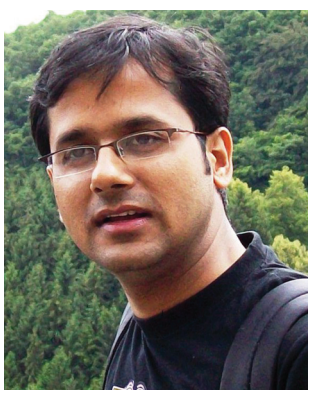

Kunal S. Mali

Kunal S. Mali obtained his Ph.D. in chemistry in 2008 from the University of Mumbai (India) under the supervision of Dr G. B. Dutt. His doctoral work focused on the investigation of fast dynamic processes in complex media by employing time-resolved fluorescence spectroscopy. Currently, he is a postdoctoral fellow at KU Leuven in the De Feyter group where his research involves various aspects of surface confined supramolecular self-assembly.

John Greenwood

John Greenwood obtained his Ph.D. in chemistry in 2013 from the University of St Andrews (UK) under the supervision of Dr Chris Baddeley. During his doctoral work he extensively studied covalent reactions on surfaces using scanning probe microscopy and vibrational spectroscopy. He joined the De Feyter group at KU Leuven in 2013 as a postdoctoral fellow, where his research involves investigating chemisorption on graphene.

to 20% of its initial length.[7] Graphene is a perfect conductor of heat exhibiting isotropic thermal conductivity exceeding 3000 W $m^{-1}K^{-1}$.[8] Despite being only one atom thick, it absorbs a rather large percentage (2.3%) of white light.[9] Moreover, graphene is completely impermeable to gases.[10] Each of the aforementioned properties warrants a technological breakthrough. Numerous potential applications have been proposed for graphene such as in high-speed radio-frequency and logic devices,[11] thermally and electrically conductive reinforced composites,[12] chemical as well as biological sensors,[13,14] desalination membranes,[15,16] photocatalysis,[17] transparent electrodes for liquid crystal displays[18] and solar cells.[19,20]

However, the translation of these astounding properties, which are often realized on tiny flakes studied in laboratories, into applications on an industrial scale suffers from some major roadblocks. Although the large-scale synthesis of graphene[21,22] has been successfully carried out recently, the mass produced material is often inferior in properties compared to pristine graphene produced by the 'scotch tape method'. There is an inherent contradiction in the properties of graphene when it comes to the realization of applications. For example, the characteristic band structure leads to an exceptionally high electron mobility thus allowing graphene transistors to process data at very high rates. But the lack of band gap also makes it difficult to turn off the flow of current – a serious impediment to logic operations. Given that such on–off switching lies at the heart of modern digital electronics, opening a small band gap in graphene has become indispensible.[23] Secondly, the handling and processing of graphene sheets is challenging since it is insoluble in most solvents. So far graphene has only been found to be soluble/dispersible in solvents with high surface tension (40–50 mJ m^{-2}) such as *N*-methyl pyrrolidone, *N*,*N*-dimethylacetamide, γ-butyrolactone and 1,3-dimethyl-2-imidazolidinone.[24] Re-aggregation into graphite-like agglomerates *via* π-stacking interactions is a looming concern even in these special solvents. The liquid-phase exfoliation of bulk graphite has been studied extensively, which involves the use of ultrasonication in the presence of intercalating compounds and/or surfactants. Although this method is up-scalable and versatile, the yield of SLG sheets is often low and requires long sonication times.[25] The insolubility of graphene in most media is not conducive for its large-scale processability thus limiting its use in various applications. Finally, the reactivity of graphene is relatively low compared to other carbon allotropes such as carbon nanotubes (CNTs) and fullerenes. Theoretically, all the sp^2-hybridized carbon atoms of graphene can undergo covalent addition reactions that convert them into sp^3-hybridized atoms. However, a strong coupling within all its p_z orbitals leads to a giant delocalized π-bonding system and thus graphene remains relatively inert. As a consequence, basal plane covalent addition usually suffer from large energy barriers necessitating the use of highly reactive species.[26–30]

One of the many ways to circumvent the above-mentioned challenges is the chemical functionalization of graphene. The surface modification of graphene can be achieved either by the physisorption of organic building blocks *via* non-covalent interactions or by the chemisorption of reactive organic species *via* covalent bond formation onto its basal plane. Both approaches have their own advantages and disadvantages. Functionalization *via* physisorption is rather mild and does not lead to the degradation of graphene properties. The availability of a virtually endless list of organic molecules makes this approach versatile. A drawback of this strategy is the limited stability of such molecular networks since they are held together by relatively weak non-covalent interactions. On the other hand, covalent bond formation between adsorbates and the carbon atoms of graphene leads to rather robust functionalization. However, since the bond formation proceeds *via* sp^2 to sp^3 rehybridization, it modifies the unique electronic band structure of graphene. Such modification is often detrimental to graphene properties, which reach their zenith only in the pristine state with perfect atomic arrangement. Furthermore, given the use of highly reactive chemical

Jinne Adisoejoso

Jinne Adisoejoso obtained his PhD in chemistry in 2012 under the supervision of Prof. Steven De Feyter at KU Leuven, studying the formation of 2D nanoporous networks. Thereafter, he moved to the Hong Kong University of Science and Technology for a postdoctoral position in the group of Prof. Nian Lin to study reactivity under ultra-high vacuum conditions. In 2014, he rejoined the group of Prof. Steven De Feyter, where his current interest involves the functionalization of graphene and other 2D materials.

Roald Phillipson

Roald Phillipson obtained his masters degree in 2013 in Nanoscience and Nanotechnology at KU Leuven (Belgium) and started his Ph.D. in the group of Steven De Feyter at KU Leuven in 2014. The main focus of his research is the functionalization of graphene for electronic applications using two-dimensional self-assembled networks.

species, spatial control over the covalent functionalization of graphene is often challenging.[26–30]

Surface functionalization can transform pristine graphene into a chemically sensitive and soluble material thus enabling its use in sensing technology[13,14] and composite materials. The covalent modification of graphene has been used to open its band gap[31,32] thus facilitating its integration into electronic devices. Since graphene has no bulk, the delocalized π electrons are heavily affected by adsorbates. As a consequence, the adsorption of organic molecules with suitably placed HOMO and LUMO levels with respect to the Fermi level of graphene is used to manipulate the type and concentration of charge carriers in graphene.[33–37] Such functionalized surfaces allow the deposition of dielectrics[38] thus creating well defined interfaces relevant for field effect transistors (FETs). Furthermore, atomic and molecular adsorption has also been used to modify the band structure in graphene thereby opening a small band gap.[39–42] Apart from these applied aspects, the organic functionalization of graphene is also intriguing from a fundamental point of view. Graphene provides an attractive test bed for comparing and contrasting the modification strategies used for similar carbon allotropes such as graphite, CNTs and fullerenes. In fact, most of the initial efforts towards graphene functionalization were based on previously well-established protocols involving graphite,[43,44] CNTs[45,46] and fullerenes.[47,48] Despite the fact that all these materials consist of sheet(s) of sp^2 hybridized carbon, significant differences exist between the properties of these allotropes and graphene. For example, suspended graphene has both its surfaces available for functionalization in contrast to graphite. On the other hand, the properties of substrate-supported graphene are significantly influenced by the underlying substrate. In addition, the high curvature of CNTs and fullerenes makes them relatively more reactive than graphene. Thus, the unique challenges and opportunities offered by the research on graphene functionalization render it a fertile area for fundamental research.

Steven De Feyter

Steven De Feyter is a professor at KU Leuven in Belgium. After completing his Ph.D. with Frans De Schryver at KU Leuven in 1997, he moved for a post-doctoral position to the group of Ahmed Zewail (California Institute of Technology, Pasadena). His research group investigates various aspects of supramolecular chemistry and the self-assembly phenomena of surfaces using scanning probe methods with special attention to liquid–solid interfaces.

In this feature article, we discuss the progress made in the field of surface supported graphene functionalization by highlighting some examples from the contemporary literature. We focus on studies where the fabrication of nanostructured graphene surfaces was targeted using well-defined organic building blocks. Surface functionalization *via* physisorption is discussed in the context of doping graphene for manipulating the charge carrier concentration and for opening a band gap. We highlight those examples where the post-functionalized graphene surface was characterized using scanning probe microscopy methods. Covalent functionalization is discussed in the context of band structure engineering. This feature article does not cover substitutional doping, which involves the replacement of carbon atoms in the honeycomb lattice of graphene by nitrogen and boron atoms.[49,50] Also, the organic functionalization of graphene in dispersions[51] is not discussed here. A number of excellent review articles published in the recent past[26–30] have summarized the influence of organic functionalization on the properties of graphene whereas MacLeod *et al.*[52] reviewed the effect of epitaxially grown graphene on the process of molecular self-assembly.

II. Non-covalent functionalization

The self-assembly of organic molecules on highly oriented pyrolytic graphite (HOPG) has been studied extensively for decades both theoretically as well as experimentally.[53,54] Given that graphite is a 3D material made up of stacked graphene layers, these previous studies are highly relevant for the non-covalent functionalization of graphene. Care has to be taken however when indulging in a direct one to one comparison between the two, since practically, graphene differs from the 'top layer' of graphite. While HOPG provides atomically flat terraces that extend several square micrometers, graphene grown on different substrates often shows a high degree of roughness and defects which arise due to the synthesis method or are inherited from the substrate underneath. Moreover, SLG is supported by either a metal or an insulator surface whereas the 'top-layer' of HOPG has an equivalent graphene layer beneath. Thus, the structure as well as the electronic properties of graphene are determined by the substrate on which it resides and thus deviate significantly from those of graphite.[55] These similarities and differences make graphene a useful new substrate that will provide additional opportunities to extend the applications of surface-confined supramolecular architectures.

The non-covalent interaction of a wide variety of molecules and materials with graphene has been studied extensively in the recent past. These include organic as well as inorganic molecules, polymers, metals, metal oxides and different types of nanoparticles.[26] In general, non-covalent interactions are sufficiently weak and thus preserve the unique electronic band structure of graphene. Moreover, the non-covalent functionalization of graphene using organic building blocks makes an otherwise inert and hydrophobic surface of graphene suitable

for secondary functionalization such as the growth of metal oxide layers. Such interfaces find important applications as dielectric layers in electronic devices[56] and as photocatalysts.[17] The research on graphene functionalization *via* molecular physisorption has mostly focused on two aspects: (1) the molecular self-assembly on graphene studied mostly from a fundamental point of view, (2) the organic functionalization of graphene for specific purposes such as doping, band-gap opening and facilitating atomic layer deposition (ALD). In the following sections we discuss the functionalization of graphene using physisorbed monolayers of organic molecules.

A. Molecular self-assembly on graphene: fundamental aspects

A number of early studies scrutinized the basics of molecular self-assembly on graphene, especially epitaxial graphene (EG) grown on SiC(0001), under ultrahigh vacuum (UHV) conditions.[57–60] The primary focus of these initial studies was to compare the assembling behavior of typical aromatic molecules on the basal plane of EG against that on HOPG and to study the influence of defects present in the EG surface on molecular self-assembly. EG/SiC remains the choice of graphene type for evaluating fundamental aspects of molecular self-assembly as it is few layers thick and typically provides relatively flat terraces in contrast to other graphene types such as chemical vapor deposited (CVD) graphene.

A large body of initial work on the molecular functionalization of substrate supported graphene was devoted to the UHV characterization of self-assembled monolayers of planar aromatic molecules using scanning tunneling microscopy (STM) and scanning tunneling spectroscopy (STS). In most of these studies, the molecule of interest was sublimed onto the graphene surface under UHV conditions. An archetypical π-conjugated molecule perylene-3,4,9,10-tetracarboxylic dianhydride (PTCDA, Fig. 1a) remains one of the most widely studied systems on graphene. Following the first low temperature STM investigation of PTCDA monolayers on bilayer graphene grown on SiC(0001) by Lauffer and co-workers,[57] Hersam and co-workers[38,58,60] have intensively studied the PTCDA-EG/SiC interface under UHV conditions. Room temperature UHV-STM measurements by Wang *et al.*[58] revealed that PTCDA forms long-range ordered, defect-free self-assembled monolayers on the surface of EG in which the molecules are packed in a herringbone arrangement (Fig. 1). PTCDA is known to assemble in an identical fashion on HOPG.[59] The molecules adsorb flat with their aromatic backbone parallel to the graphene surface due to π stacking interactions. The intermolecular interactions are dominated by aromatic C–H···O–C hydrogen bonds.

An important facet of the PTCDA self-assembly on graphene which differs from that on HOPG is the behavior of the self-assembled network at the step edges. In the case of HOPG, the network is typically discontinuous across a step-edge.[59] In other words, a step edge on HOPG interrupts the molecular domain and each terrace comprises of a separate domain. In contrast, PTCDA networks were found to be in full compliance with the underlying graphene topology and thus seamlessly

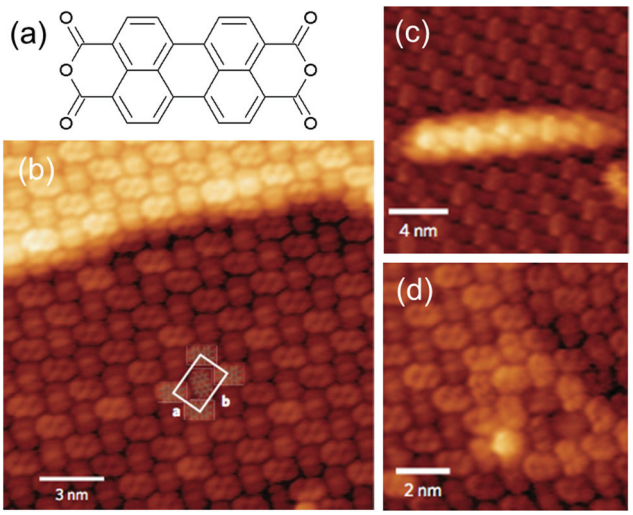

Fig. 1 Functionalization of EG/SiC using the physisorbed PTCDA monolayer. (a) Molecular structure of PTCDA. (b) High-resolution STM image of the PTCDA monolayer on EG/SiC. The monolayer continuously follows the graphene sheet despite the presence of step-edge in the underlying SiC substrate. (c) PTCDA monolayer covering a graphene-subsurface nanotube defect. (d) Another type of defect, namely a six-fold scattering-center defect, is also unable to disrupt the regular arrangement of PTCDA molecules. Reprinted with permission.[58] (Copyright © 2009 Nature Publishing Group.)

crossed surface steps (Fig. 1b), which are inherited by the underlying SiC substrate. This peculiar aspect of self-assembly on graphene was confirmed later for a number of other systems such as the densely packed networks of phthalocyanines,[61] pentacosadiynoic acid (PCDA)[62] and the low density networks of dehydrobenzo[12]annulene (DBA) derivatives.[63] These findings indicate that the formation of continuous domains over the step-edges is not a property of a given molecular system but is rather inherent to the graphene–substrate combination since rigid polycyclic aromatic (PTCDA, phthalocyanines) as well as flexible alkyl substituted (PCDA, DBA) molecules exhibit identical behavior upon adsorption on graphene.

The PTCDA monolayers were found to be unaffected by the intrinsic defects present in the EG passing unperturbed over the subsurface nanotubes and six-fold scattering centers (Fig. 1c and d). Furthermore, in contrast to HOPG, where the molecular domains are typically oriented at multiples of 60° with respect to each other, the PTCDA domains on EG/SiC were found to be rotated by arbitrary orientations. This finding however was contested later by Huang *et al.*[59] in another low temperature UHV-STM investigation, which revealed the existence of typical 60° orientations within the PTCDA domains. STS experiments suggested that the electronic structure of PTCDA remains unperturbed upon adsorption on EG/SiC thus implying only weak coupling with the underlying graphene layer.[57–59] While the low temperature experiments[57,59] revealed weak electron transfer from graphene to the PTCDA monolayer, such n-type charge transfer doping was found to diminish upon approaching room temperature.[58] The robust PTCDA

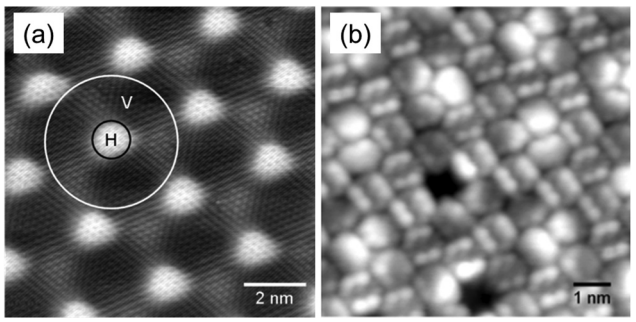

Fig. 2 Influence of the moiré superstructure of graphene on PTCDA self-assembly. (a) Atomically resolved STM image showing the moiré superstructure of EG/Ru(0001). 'H' stands for 'hills' and 'V' indicates the 'valleys' in the moiré corrugation. (b) STM image of the PTCDA monolayer on EG/Ru(0001). Missing molecule defects are often found on the bright 'H' sites. Reproduced according to the Creative Commons license.[68]

adlayer on EG/SiC was further used as a chemical resist to create sub-5 nm shallow nanopatterns which were later filled with PTCDI molecules thus giving rise to heteromolecular organic nanostructures on EG/SiC.[60] Such deposition protocols that yield spatially periodic molecular patterns at the sub-5 nm length scale in registry with the graphene surface are considered to be desirable for the band structure modification of graphene without degrading its charge carrier mobility.[64,65]

Superposition of the graphene lattice with that of the substrate often gives rise to an interference effect known as the moiré pattern. This pattern defines a superlattice, which has a periodicity larger than that of either of the individual lattices. When the carbon atoms in the graphene lattice reside over the substrate atoms, the graphene–substrate electronic interaction is maximized. Such regions in the moiré pattern appear dark in STM images due to the reduced density of states near the Fermi level. The bright regions in contrast appear in areas where the carbon atoms rest above the hollow sites (fcc as well as hcp) in the underlying substrate lattice (Fig. 2a). The moiré superlattice imparts structural and electronic modulation thus creating a spatially varying potential landscape on the graphene surface. Recent theoretical and experimental data have shown that the observed buckling on Ru(0001) is not only an electronic effect in the STM image, but in fact reflects a real height corrugation of 1.5 Å.[66] The influence of such a superlattice on molecular self-assembly can be negligible or significant depending on whether the interaction of graphene with the underlying substrate is weak or strong, respectively. EG has weak interactions with substrates such as Ir(111) and SiC(0001) whereas it interacts strongly with Ru(0001) and Ni(111).[67] Consequently, graphene presents a much more HOPG like adsorption landscape when grown on weakly interacting substrates. On the other hand, the moiré superlattice on strongly interacting substrates has been shown to influence molecular adsorption, especially at low temperatures.

The influence of graphene superlattice on molecular adsorption has been well documented[52] and is reported for PTCDA as well. The herringbone films of PTCDA formed on EG/Ru(0001) show missing molecule defects which are located on top of the bright (H) sites in the graphene moiré pattern (Fig. 2). This effect was ascribed to the pronounced variation in the surface electronic structure imparted by the moiré pattern, which leads to lateral modulation in the adsorption potential along the graphene surface. The influence of moiré corrugation was found to be even more drastic in the case of 2-phenyl-4,6-bis(6-(pyridin-3-yl)-4-(pyridin-3-yl)pyridin-2-yl)-pyrimidine (3,3′-BTP, Fig. 3a) and 2,4′-bis(terpyridine)(2,4′-BTP, Fig. 3d) adsorption. These two molecules form supramolecular networks based on C–H···N type hydrogen bonding. Due to the different locations of nitrogen atoms within the molecular backbone, the two molecules are known to form fundamentally different supramolecular structures.[69,70] The adsorption of 3,3′-BTP on EG/Ru(0001) however resulted in the formation of multiple random architectures that include triangular, circular and linear structures (Fig. 3b) wherein the molecules exclusively occupied the 'valley' sites while most of the bright 'hill' sites remained vacant. This behavior is in stark contrast to that observed on HOPG, wherein long-range ordered 2D monolayers were obtained.[69] The peculiar adsorption behavior on EG/Ru(0001) was explained using force field calculations, which revealed a difference of the order of −0.625 to −0.985 eV per molecule in the adsorption energy between the 'hill' and 'valley' sites.[68] 2,4′-BTP, on the other hand, formed hydrogen bonded 1D chains on EG/Ru(0001) (Fig. 3e) due to the appropriately placed N atoms on the molecular backbone. STM images revealed that similar to 3,3′-BTP, the linear chains formed by 2,4′-BTP selectively occupied the valley sites. The energetic preference for adsorption in the valley sites was explained once again using force field calculations, which revealed that the hill sites offer weaker adsorption sites (E_{hill} = −3.45 eV) compared to the valley sites (E_{valley} = −4.08 eV). The authors also noted that the total intermolecular interaction energy of the extended BTP networks on HOPG is much smaller than the pronounced energy variation within the moiré corrugation.[71]

Although molecular self-assembly has been extensively studied on EG, CVD graphene grown on copper (CVD-G/Cu) has garnered significant attention in the recent past. The reason behind the rapidly increasing popularity of such graphene type is its mass producibility and a relatively cheaper production cost compared to EG. Typically, CVD graphene is grown on polycrystalline copper foils which can then be transferred to a variety of different substrates making this graphene type an attractive platform for various applications.[72] The most commonly used insulating substrate for transferred graphene is SiO_2. While the surface roughness of graphene on SiO_2 is relatively high with the corrugation amplitude reaching almost 1 nm, this combination nevertheless is being extensively studied due to the importance of SiO_2 in the existing semiconductor technology. The molecular functionalization of CVD graphene has been examined both under UHV as well as ambient conditions. Some research groups have investigated self-assembly on CVD graphene grown on Cu foils,[61,73] while

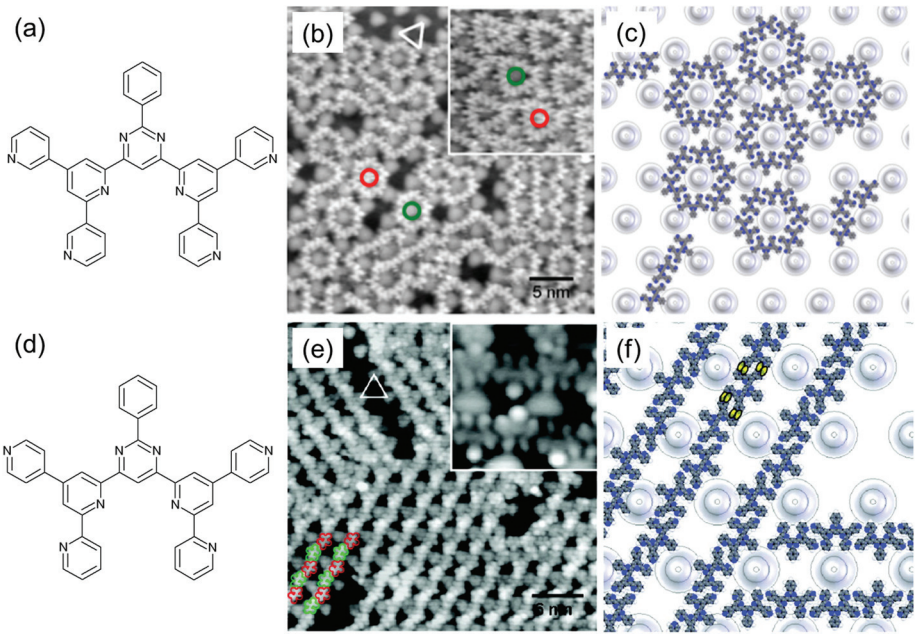

Fig. 3 Influence of the moiré superstructure on the self-assembly of 3,3′-BTP (a) and 2,4′-BTP (d). (b) STM image of 3,3′-BTP physisorbed on the EG/Ru(0001) surface. Within the different supramolecular structures formed, 3,3′-BTP molecules avoid adsorption onto the hill sites of the moiré corrugation as shown in (c). (e) 2,4′-BTP monolayer on EG/Ru(0001) also shows preferential adsorption in the valley sites as shown in (f). Panels (b) and (c) are reproduced according to the Creative Commons license.[68] (e) and (f) Reprinted with permission.[71] (Copyright © 2011 American Chemical Society.)

others have used CVD graphene transferred on SiO_2 or hexagonal boron nitride (h-BN).[74]

Phthalocyanines constitute another class of planar aromatic compounds that have been studied in depth on epitaxial graphene grown on metal substrates such as Ru(0001),[75,76] Ni(111),[77] Ir(111)[78] as well as on SiC.[79] In these studies also, the self-assembled structures were correlated with the moiré corrugation of the graphene surface, which provide trapping sites for molecules. One of the notable findings is the observed preferential adsorption of copper hexadecafluoro-phthalocyanine (F16CuPc) on SLG in the presence of bilayer graphene when the adsorption experiments were carried out on EG/SiC.[79] Only when the SLG terraces were fully occupied, the F16CuPc molecules were found to start adsorption on bilayer graphene terraces. This peculiar behavior arises due to a subtle difference in the electronic structure of SLG and bilayer graphene, which in turn affects the adsorption energies. First principles calculations revealed that the adsorption energy of F16CuPc on SLG is 0.3 eV higher than that on bilayer graphene.

Järvinen *et al.* compared the self-assembly behavior of cobalt phthalocyanine (CoPc) on CVD grown graphene transferred onto SiO_2 and h-BN using low temperature UHV-STM.[74] While CoPc formed a square lattice on both the substrates, the assembly behavior at the level of domains was found to be drastically different. The CoPc domains were interrupted by the corrugation of CVD graphene whereas adsorption on G/h-BN led to the formation of flawless domains that extended over the entire terraces of the underlying h-BN. Interestingly, the moiré pattern of h-BN did not affect the adsorption behavior of CoPc thus suggesting the possibility of achieving single domain molecular layers on the device scale. The authors concluded that graphene on h-BN is an ideal substrate for molecular self-assembly in the context of controlling the electronic properties of graphene *via* engineered potential landscapes (Fig. 4).[74]

Although a majority of molecular self-assembly experiments on surface supported graphene have been carried out under UHV environments, increasing attention is being paid to the development of functionalization protocols that work under ambient conditions. Typically, such a procedure involves bringing the molecules in contact with the graphene surface in an organic solvent. Such a solution processing approach has the advantage of scalability over the often-used UHV deposition method *via* sublimation. Apart from being a straightforward experimental approach, self-assembly at the organic liquid–solid interface[54] also relaxes the upper limit on the molecular weight of the compounds that can be used for functionalization, since the sublimation of higher molecular weight compounds is often challenging. The solution based deposition approach is expected to gain popularity as it is rapid and can build on the wealth of information already available from numerous studies carried out at the organic solution–HOPG interface.[80] Although only a few in number so far, reports describing the functionalization of graphene under ambient conditions indicate that the liquid–solid interface

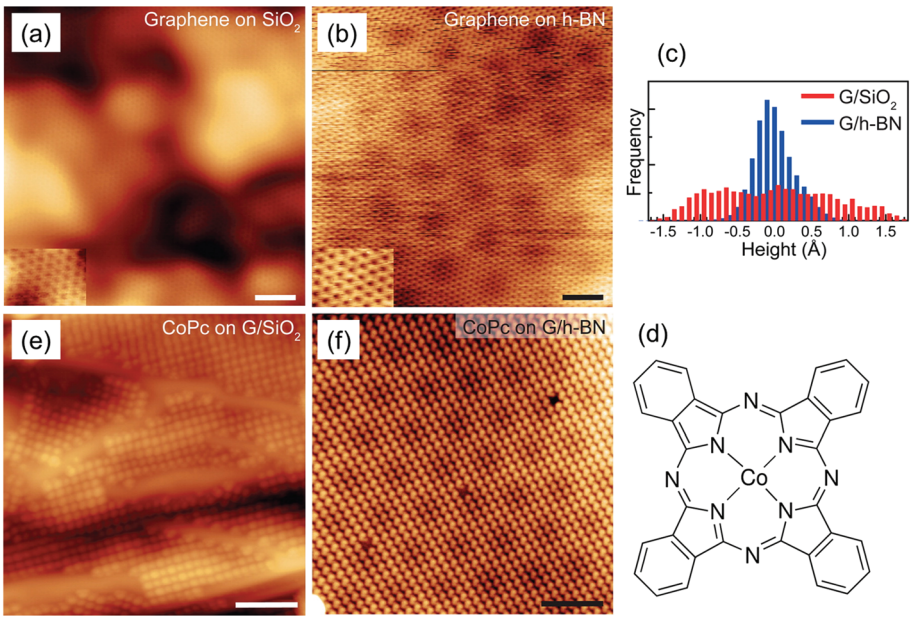

Fig. 4 Comparison of CoPc adsorption on CVD graphene transferred onto SiO_2 and h-BN. (a) and (b) show the STM images of CVD-G/SiO_2 and CVD-G/h-BN, respectively, before the deposition of molecules. (c) Height histograms obtained from the STM images are shown in panels (a) and (b) indicating that CVD-G/h-BN offers a relatively smooth surface compared to that on SiO_2. (d) Molecular structure of CoPc. (e) and (f) show the representative STM images of the CoPc monolayer on CVD-G/SiO_2 and CVD-G/h-BN, respectively. Reprinted with permission.[74] (Copyright © 2013, American Chemical Society.)

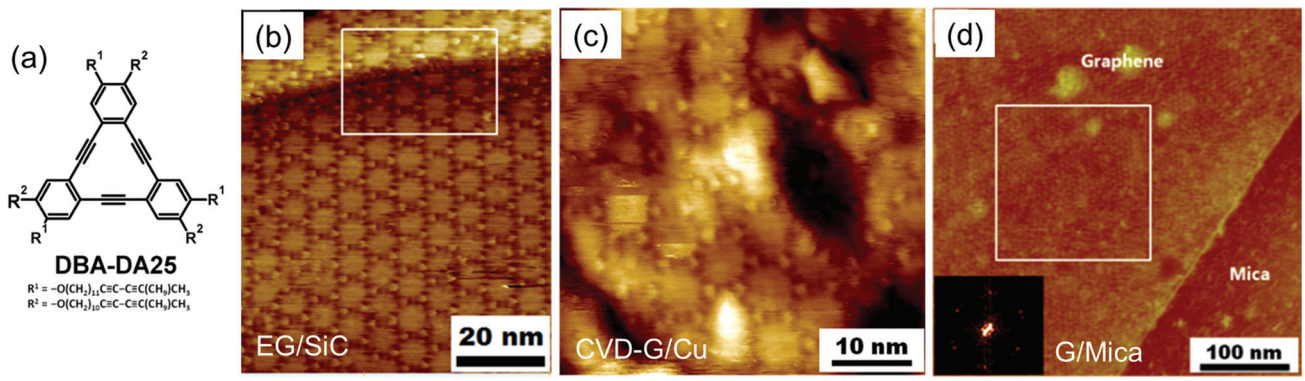

Fig. 5 DBA-DA25 self-assembly on different types of graphene substrates. (a) Molecular structure of DBA-DA25. Porous supramolecular networks of DBA-DA25 formed on (b) EG/SiC, (c) CVD-G/Cu and (d) exfoliated graphene on mica using solution deposition under ambient conditions. Reprinted with permission.[63] (Copyright © 2013, American Chemical Society.)

is an interesting medium for constructing ordered supramolecular networks on graphene and holds promise for large-scale functionalization.

Li *et al.* were one of the first to capitalize on molecular self-assembly at the organic solution–graphene interface. The network formation of a DBA derivative possessing long alkoxy chains containing diacetylene units (DBA-DA25, Fig. 5a) was investigated on different types of graphene namely, EG/SiC, CVD-G/Cu and exfoliated graphene on mica using a combination of STM and AFM.[63] DBA-DA25 formed stable self-assembled networks on all three types of graphene substrates (Fig. 5b and c). In contrast to most of the previous reports that dealt with densely packed molecular layers, the DBA-DA25 self-assembly furnished porous networks that exposed the pristine graphene surface in a spatially repetitive fashion at the nanoscale. The networks are sustained by van der Waals interaction between interdigitating alkyl chains that show the same type of epitaxial relationship with graphene as they do with HOPG. In line with UHV studies that were mostly carried out on rigid polycyclic aromatic compounds, the relatively flexible DBA-DA25 networks also conform to the steps and wrinkles on the graphene surface. Furthermore, these monolayer thick films were found to be stable in liquids as well as upon prolonged exposure to ambient air. The low-density

DBA-DA25 monolayers are promising for carrying out the secondary functionalization of graphene using other molecules that can adsorb within the voids, thus invoking applicability in sensing. This investigation not only identified a robust molecular system that survives washing/drying under ambient conditions but also provided a much-needed comparison of the self-assembly of a single building block on graphene supported by different substrates.[63] To date this remains only one of the three porous supramolecular systems assembled on graphene, the other two being bimolecular porous networks of melamine-PTCDI prepared under UHV on EG-SiC reported by Karmel *et al.*[81] and trimesic acid monolayers on graphene/SiO_2 studied under ambient conditions by Zhou *et al.*[82]

An intriguing structural facet of the porous networks of DBA-DA25 is the presence of diacetylene units that can undergo light-induced polymerization[83] to yield robust porous networks in which the molecules are connected to each other *via* covalent bonds. While this is an exciting possibility and can be explored in the context of graphene functionalization, such so called 'covalent organic frameworks' (COFs) are routinely synthesized for their use in gas storage, photonic and catalytic applications. COFs are a class of highly crystalline porous materials and their cavity size can be tuned with nanometer accuracy. The 2D variants of such materials, 2D COFs, are appealing for graphene functionalization due to their robustness relative to the supramolecularly assembled structures. A major drawback however is that a majority of COFs are synthesized as bulk powders and therefore their controlled deposition on graphene remains a challenge.[84]

An attractive alternative is to carry out the synthesis of 2D COFs in the presence of graphene so that the layered material gets deposited on graphene as it is formed in solution. Colson *et al.* used this strategy to functionalize SLG supported by different substrates such as Cu, SiC and transparent fused silica with COFs. Boronic acid chemistry was used under solvothermal conditions to synthesise 2D COFs in the presence of SLG. The coverage and thickness of the COF films was evaluated by scanning electron microscopy, which showed the complete coverage of SLG but indicated the formation of thick films that correspond to a few hundred layers of COF. Grazing incidence diffraction measurements confirmed the formation of highly crystalline materials in which the hexagonal pores are aligned orthogonally to graphene.[85] The thickness of the film may constitute a challenge in using such COF functionalized graphene in top gated FETs. Limiting the concentration of precursors available at the solution–graphene interface can in principle circumvent this problem and yield monolayer thick COFs on graphene. A recent noteworthy example in this context is the demonstration of monolayer COF formation on graphene. Using a purely surface science approach, Xu *et al.* achieved the decoration of CVD-G/Cu with a 2D COF obtained using Schiff base chemistry. STM measurements confirmed the formation of porous COF on the graphene surface.[86] While numerous exciting possibilities exist for functionalization of graphene using COFs, this area remains largely unexplored.

B. Non-covalent functionalization of graphene: doping *via* physisorption

An important motivation behind studying molecular assembly on graphene has been the prospect of opening a band gap in graphene, which is otherwise a semi-metal, as well as to achieve precise control over the charge carrier type (p- or n-type) and density. Graphene can be doped by adsorption of gases, certain alkali atoms such as potassium, organic molecules and also by the substrate on which it resides. Under ambient conditions there is always some degree of p-type doping due to the adsorption of water and molecular oxygen.[87] The doping upon gas adsorption has been utilized in gas sensors which show extremely low detection limits, down to the single molecule level.[88] Alkali atoms, such as potassium, are very strong electron donors and form ionic bonds resulting in n-type doping of graphene.[89] The distribution of metal atoms however, is often inhomogeneous and the charge carrier mobility degrades upon adsorption due to an increased charged-impurity scattering.[90]

Apart from the aforementioned dopants, the solid substrate that supports graphene also influences its band structure. Typical substrates such as SiC, SiO_2 and different metals are known to modify the band structure of graphene *via* electronic coupling.[91,92] However, the type and extent of charge carrier modification in each case depends on the specific preparation conditions and thus it is difficult to predict. In view of the challenges associated with controlling/tuning the extent of doping exerted by gases, metal atoms and substrates, doping by the physisorption of organic molecules is considered superior as it allows precise control over molecular organization using well-established principles of supramolecular chemistry. Due to the large specific surface area of a graphene sheet, the electronic influence of the adsorbed molecules becomes significant, providing a simple, effective and non-destructive way to tailor the band structure of graphene.

Besides weak dispersive interactions, organic molecules possessing electron withdrawing or donating functional groups can have strong charge transfer interactions with graphene thus leading to its doping. This type of doping takes place *via* charge transfer from the adsorbed dopant (graphene) to graphene (dopant). Whether the charge transfer will take place is determined by the relative position of density of states (DOS) of the highest occupied molecular orbital (HOMO) and the lowest unoccupied molecular orbital (LUMO) of the dopant and the Fermi level of graphene (Scheme 1). Charge is transferred from the dopant to the graphene layer, if the HOMO of the dopant is above the Fermi level of graphene resulting in n-type doping. On the other hand, for dopants with LUMO below the Fermi level of graphene, charge transfer occurs from the graphene layer to the dopant amounting to p-type doping. p-Type doping drives the Dirac point of graphene above the Fermi level, and n-type doping drives the Dirac point below the Fermi level. Apart from the exact separation of the HOMO/LUMO levels of the dopants with respect to the Dirac point of graphene, the amount of charge transferred per molecule also

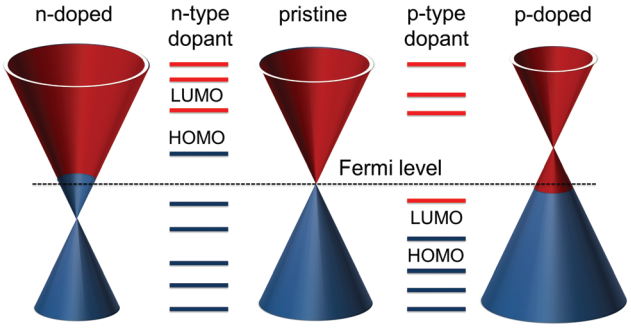

Scheme 1 A schematic showing the relationship between positions of the HOMO–LUMO levels of dopants with respect to the Fermi level of graphene relevant for n- and p-type doping of graphene (see text for details).

depends on the orientation and distance of the adsorbate with respect to the graphene plane.

Tetrafluoro-tetracyanoquinodimethane (F4-TCNQ), a strong electron acceptor, remains one of the most intensively studied organic dopants on graphene.[35,36,93,94] The electron affinity of F4-TCNQ is 5.24 eV and thus its LUMO lies well below the Dirac point of graphene. Chen *et al.*[35] first demonstrated the utility of F4-TCNQ for p-doping EG/SiC. The charge transfer between thin films of F4-TCNQ and EG/SiC was studied using synchrotron-based high-resolution photoemission spectroscopy (PES). Photoemission spectra revealed electron transfer from EG/SiC to the F4-TCNQ layer, which is consistent with the strong electron withdrawing nature of F4-TCNQ. In other words, an electron rich layer accumulates in the F4-TCNQ adlayer whereas an electron depleted layer is localized on the other side of the interface in EG/SiC thus effectively doping the graphene with holes. Coletti *et al.*[36] approached the F4-TCNQ/EG system from a different perspective. They reasoned that the strong p-doping effect of F4-TCNQ could be used to negate the n-type doping exerted by the underlying SiC substrate. Angle resolved photoemission spectroscopy (ARPES), which measures the distribution of electrons in reciprocal space, provided direct evidence for the negative charge compensation of EG/SiC by F4-TCNQ. A gradual increase in the F4-TCNQ layer thickness revealed the complete neutralization of substrate-induced n-type doping at a thickness of 0.8 nm. Both the studies revealed saturation in the work function after a certain film thickness was reached, indicating that the electron transfer occurs only at the F4-TCNQ–graphene interface whereas the bulk of the film remains uncharged.[35,36]

p-Type doping of graphene has also been accomplished under ambient conditions *via* solution based deposition of organic molecules. Prado *et al.*[95] scrutinized the assembling behavior as well as the doping capability of long chain alkylphosphonic acids using a combination of AFM, Raman spectroscopy and first principles calculations. 2D crystals of these compounds were formed by dropcasting ethanol solutions on mechanically exfoliated graphene flakes supported by SiO_2, followed by the evaporation of the solvent. AFM revealed well-ordered striped domains of tetradecyl- as well as octadecylphosphonic acid (OPA, Fig. 6a and b) on exfoliated graphene. Raman spectroscopy analysis of the flake deposited with octadecylphosphonic acid further revealed that the position of the G peak of graphene shifts to higher wavenumbers and also the full width at half maximum of this peak is reduced compared to the pristine graphene flake. Moreover, the ratio of peak intensities of the G and 2D peaks was reduced by 60% upon deposition of OPA further corroborating electron transfer from graphene to the phosphonic acid monolayer, which effectively p-dopes graphene (Fig. 6c). The assembly structure as well the doping effect was corroborated by first principles calculations.[95]

In a slightly different approach, alkylthiol monolayers, which adsorb in an identical fashion to alkylphosphonic acids on graphene, were used to realize the sensing capabilities of the organic monolayer–graphene interface. Zhang *et al.*[96] functionalized GFETs prepared from exfoliated graphene flakes with 1-octadecanethiol using spin coating of a chloroform solution. Given the high affinity of thiol groups towards mercury, the well-ordered self-assembled networks of 1-octadecanethiol could be used for capturing mercury ions from a

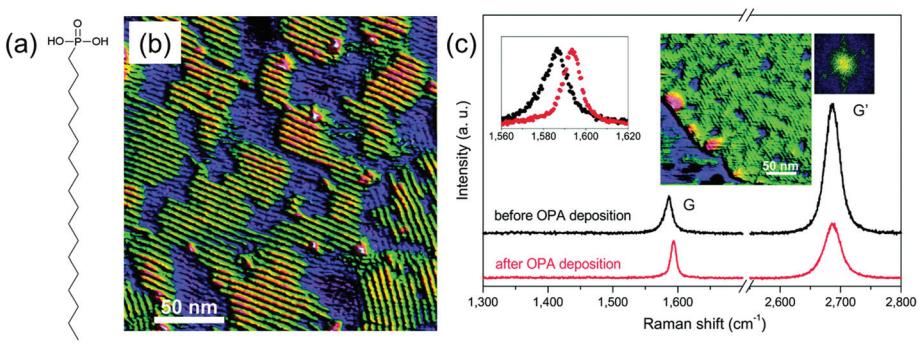

Fig. 6 Charge transfer doping (p-type) of exfoliated graphene using alkylphosphonic acids. (a) Molecular structure of OPA. (b) AFM topography image of the OPA self-assembled network (yellow-green) that partially covers the graphene flake (blue). (c) Raman spectra obtained on the graphene flake before and after OPA functionalization illustrating p-type doping. Reproduced with permission.[95] (Copyright © 2011 American Chemical Society.)

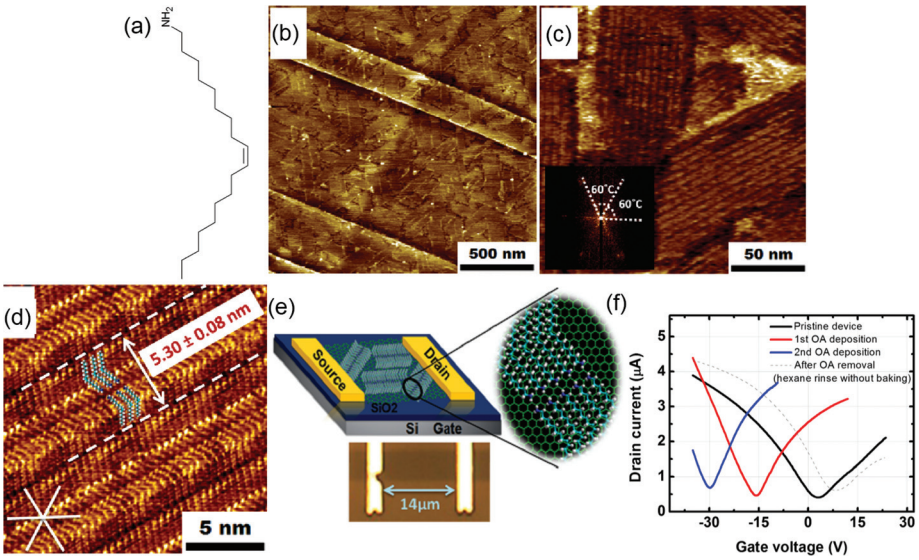

Fig. 7 Charge transfer doping (n-type) of exfoliated graphene using oleylamine. (a) Molecular structure of oleylamine. (b) and (c) show large- and small-scale AFM images of oleylamine monolayers adsorbed on HOPG. (d) Molecular resolution STM image of oleylamine on HOPG. (e) A schematic showing the graphene device decorated with the oleylamine monolayer. Lower half of the panel (e) shows the optical micrograph of the GFET. (f) I_{ds}–V_g characteristics of a graphene FET device before and after several OA treatments and after OA removal taken at a source–drain bias (V_{ds}) of 5 mV under ambient conditions. Reproduced with permission.[37] (Copyright © 2013 Royal Society of Chemistry.)

solution. The incorporation of the mercury ions in the monolayer resulted in a measurable shift of the charge neutrality point to more positive potentials due to p-type doping.

Given the relatively low work function of graphene (−4.6 eV), n-type doping is perceived to be more challenging than p-type. A noteworthy example is that of the self-assembled monolayers of *cis*-1-amino-9-octadecene, a molecule commonly referred to as oleylamine (Fig. 7a). This molecular system consists of an electron rich primary amino group that serves as the n-type dopant whereas the long alkyl chain facilitates its adsorption onto graphene. A combination of STM, AFM and electrical characterization of GFETs was used to assess the adsorption behavior and n-doping effect of oleylamine. AFM and STM revealed large area, well-ordered self-assembled monolayers of oleylamine on HOPG (Fig. 7b–d) and EG/SiC. Back-gated GFETs made from exfoliated graphene (Fig. 7e) were functionalized with oleylamine using an identical deposition protocol. Electron accumulation in the graphene channel was found to increase upon adsorption of oleylamine which essentially amounts to n-type doping. The n-type doping achieved upon deposition of approximately one monolayer could be improved further upon an additional second deposition on the device (Fig. 7f). The functionalized devices were stable and the doping levels as well as the carrier mobilities remained constant upon exposure to high vacuum conditions for a prolonged period confirming the robustness of the deposit. An important aspect of this investigation is that the pristine device characteristics could be regained by sonication of the device in hexane showing that electron doping by oleylamine can be reversed. This study highlighted the important relationship between the molecular structure, the supramolecular ordering of the dopant on the graphene surface and the resulting device performance of GFETs.[37]

Zhou *et al.* targeted local n-type doping by patterning exfoliated graphene with rhodamine 6G (R6G) using dip-pen nanolithography (DPN). DPN is a scanning probe lithography technique in which an AFM tip is used to transfer molecules onto substrates of interest to create patterns in a well-defined fashion. Narrow lines of R6G were 'written' on top of exfoliated graphene supported by SiO_2. A comparison of back-gate field-effect measurements on two terminal graphene devices before and after bulk functionalization with R6G revealed a shift of the Dirac point to negative gate voltages indicating n-type doping. Raman spectroscopy measurements were used to corroborate the electrical measurements. The local doping effect by narrow R6G lines was further confirmed by employing Kelvin probe force microscopy (KPFM) – another scanning probe technique that measures the contact potential difference (CPD) between the surface and the conducting AFM probe. KPFM measurements revealed a decrease in the CPD when measured over R6G lines relative to the pristine graphene surface, confirming the localized nature of the n-doping effect.[97] n-Type doping of graphene has also been accomplished using physisorption of other molecules such as saturated alkylamines,[98] 1,5-naphthalenediamine, 9,10-dimethylanthracene,[34] and *p*-toluenesulfonic acid.[99]

C. Non-covalent functionalization of graphene: band gap opening

One of the illustrious properties of graphene, its excellent charge carrier mobility, is not perceived as its most compelling feature by the electronic-device community, in part due to its

semi-metallic nature.[23] The integration of graphene into various electronic and photonic applications necessitates the opening of an electronic band gap. Attempts to open a bandgap in graphene have been mostly centered around three approaches: (1) confining graphene in one dimension to form graphene nanoribbons (GNRs).[100] (2) biasing bilayer graphene[101] and (3) applying strain to graphene.[102] The first approach has stimulated a lot of interest in the chemistry community as the well-established principles of synthetic polymer chemistry can be put to test to produce such narrow GNRs. In fact, Narita *et al.* recently demonstrated the solution phase bottom-up synthesis of long (>200 nm) GNRs with a large bandgap of 1.88 eV.[103] While the bottom-up approach to GNRs is promising, the scalability of GNR synthesis as well as the incorporation of such materials in devices remains largely unexplored. Apart from the three strategies mentioned above, molecular functionalization can also be used to open a band gap in graphene. The covalent attachment of molecules to the basal plane of graphene, which is described later in this article, has been used for opening a band gap in graphene. In the following paragraphs we discuss the experiments that targeted band gap opening using molecular physisorption.

Band gap engineering *via* physisorption of organic molecules has been reported for both bilayer and monolayer graphene. In bilayer graphene the two graphene layers are typically Bernal (AB) stacked and just like SLG, pristine Bernal stacked bilayer graphene is also a gapless semiconductor. However, when an external electric field is applied normal to the graphene plane, a band gap is opened due to the breaking of the inversion symmetry between the layers.[101] Similarly, a band gap is also opened by an interlayer electric field induced by molecular dopants adsorbed on the bilayer graphene surface[41] and therefore, the strategies for doping graphene discussed in the previous section could as well be applied for opening a band gap in bilayer graphene. Self-assembly in conjunction with opening the band gap of graphene has not been experimentally demonstrated yet, though a few research groups have attempted band gap engineering using organic adsorbates.

Zhang *et al.* used thin layers of triazine thermally evaporated on exfoliated bilayer graphene to open an electrical band gap and improve the on–off characteristics of GFETs.[41] The band-gap opening was linearly proportional to the amount of doping and varied as 70 meV/10^{13} cm^{-2}, resulting in a band gap of ≈111 meV at the maximum doping concentration. A notable aspect of this investigation is that the improvement in the on/off ratio was critically dependent on the exposure to ambient air. Blocking the access of air/moisture to the bottom layer of bilayer graphene (interface of graphene with SiO_2) led to a decrease in the on/off ratio, which indicated that ambient p-type doping by oxygen or water plays a crucial role in the creation of charge asymmetry between the top and the bottom layers. This gap nevertheless is still far from the desired minimum (0.4 eV)[23] and resulted therefore, only in a limited improvement of the on/off ratio. Thus the selection of dopants is crucial for the improvement of the on/off ratio of GFETS since the band gap opening is limited by the doping concentration.

The sensitivity of the graphene band structure to the lattice symmetry has been exploited to open a band gap in SLG using controlled adsorption of water molecules. Yavari *et al.* measured temperature dependent transport properties of SLG in an atmospheric chamber with a precise control of humidity. By extracting the activation energy from *T*-dependent conductivity plots, they could indirectly infer the opening of a band gap of up to 0.206 eV. The band gap opening in this case was speculated to be a result of breaking of the sub-lattice symmetry due to the adsorption of water. The authors claim that the adsorption of water molecules both above the graphene surface as well as in between the graphene and the SiC substrate leads to the breaking of the chemical equivalency of the A and B sites in graphene consequently reducing the symmetry at the Dirac point. Theoretical aspects of band gap formation in graphene through such sub-lattice modification have been recently reviewed.[104] It must be noted however, that so far only limited experimental evidence is available that proves the creation of a sizeable band gap in SLG using molecular physisorption.[39]

D. Molecular self-assembly on graphene: atomic layer deposition

FET constitutes a major workhorse in the modern semiconductor industry. Most work carried out on graphene devices to date relates to FETs. The integration of graphene into FETs often requires the growth of a high dielectric constant (high-*k*) material such as SiO_2, Al_2O_3 or HfO_2 that acts as the top gate insulator. The performance of a FET often critically depends on the quality of these high-*k* films, which are expected to be ultrathin, uniform and pinhole free. ALD is a preferred thin film technique used for the deposition of high-*k* materials, which employs self-limiting sequential surface chemistry to enable atomic scale control over the deposition of thin films.[105] However, ALD on pristine graphene is challenging due to its inert and hydrophobic nature resulting in poor-quality, non-uniform and leaky films which lead to sub-optimal electrical performance.[56]

Several surface pretreatment strategies have been suggested to improve the ALD film quality. These include the deposition and oxidation of metal films on graphene prior to ALD,[106] the oxidation of graphene using ozone[107] and spin coating of polymer films[108] as a seeding layer. However, the former two approaches damage graphene and result in the degradation of its electronic properties, while spin coating of polymers is difficult to control in terms of layer thickness, surface coverage and density of nucleation sites. Moreover, due to the increased gate thickness and a reduced effective *k* value, these polymer layers decrease the overall capacitance of the gate dielectric layer.[108] As a result, molecular physisorption has been explored as a surface modification protocol for rendering graphene suitable for ALD growth without increasing the gate thickness significantly.

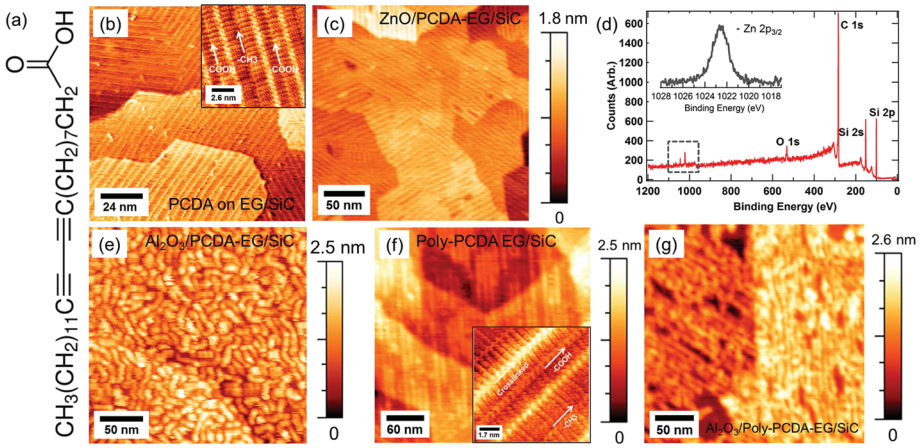

Fig. 8 Physisorbed monolayers for ALD of ZnO and Al_2O_3 on EG/SiC. (a) Molecular structure of PCDA. (b) STM image of the PCDA monolayer on EG/SiC. Inset shows the high resolution STM image. (c) AFM image of the PCDA modified graphene surface after ZnO deposition. (d) XPS spectrum obtained after ALD of ZnO showing the presence of Zn. (e) AFM image showing a non-uniform lamellar morphology of the PCDA-EG/SiC surface after the deposition of Al_2O_3. (f) AFM image of the monolayer after photopolymerisation of PCDA molecules. The inset shows high-resolution STM; a cross-linked strand can be seen together with another strand where polymerization has not occurred. (g) AFM image showing uniform deposition of Al_2O_3 films obtained on polymerized PCDA monolayers. Reproduced with permission.[109] (Copyright © 2013 American Chemical Society.)

Dai *et al.* delineated the challenges associated with ALD of metal oxides on pristine graphene. ALD of Al_2O_3 on graphene flakes on SiO_2 revealed that growth of the oxide layer occurs only at the edges of the graphene flake or defects on the basal plane since pristine graphene lacks dangling bonds or any other surface functionality.[56] The selectivity of ALD growth on defect sites was proposed as a simple tool to locate surface defects on the graphene basal plane. The flakes were then functionalized with 3,4,9,10-perylene tetracarboxylic (PTCA) acid by dip coating to achieve the uniform growth of Al_2O_3. ALD on such PTCA functionalized flakes revealed the formation of uniform ultrathin Al_2O_3 deposition on graphene thought to be facilitated by the carboxylate groups of PTCA that serve as nucleation sites for ALD.

The functionalization strategy to facilitate ALD was then intensively explored by Alaboson *et al.* who used well-ordered self-assembled networks of organic molecules on EG/SiC. Monolayers of aromatic (PTCDA) as well as aliphatic (PCDA, Fig. 8a) compounds were used for the nucleation of ALD precursor species on graphene. Smooth and highly uniform films of HfO_2 and Al_2O_3 could be obtained on EG/SiC functionalized with PTCDA.[38] Adhesion and inherent stability of the dielectric films were confirmed by contact conductive AFM measurements. Specular X-ray reflectivity further revealed that the underlying PTCDA monolayer remains structurally intact in terms of layer occupation and stacking after the ALD process. Parallel-plate metal-oxide-graphene capacitors fabricated using PTCDA modified graphene exhibited high capacitance and low leakage currents.

The versatility of this approach for ALD growth was demonstrated using PCDA monolayers that consist of long alkyl chains with carboxyl groups. PCDA modified EG/SiC could be efficiently coated with uniform ZnO as well as with Al_2O_3 films (Fig. 8).[109] Grazing incidence small/wide angle X-ray scattering confirmed that Zn coordinates with the neighboring carboxylate groups of the adjacent PCDA molecules forming ZnO chains, which are oriented along specific graphene lattice directions. In contrast, the growth of Al_2O_3 (using trimethyl aluminium, TMA) was found to be continuous but disordered. It was observed that TMA attacks and removes the acetylene group of the PCDA molecules, the principal contribution to the monolayer stability. The quality of Al_2O_3 films grown on PCDA modified graphene was improved by the photochemical crosslinking of PCDA molecules with UV light[62] which allowed for more ordered and thicker films.

III. Covalent functionalization

Physical engineering methods such as lithography have severe limitations when it comes to the large scale processing of graphene and thus the precise molecular level modification of graphene falls within the realm of organic chemistry. The covalent attachment of organic molecules onto the basal plane of graphene is an intensively researched area and is often perceived as a relatively more robust approach towards graphene functionalization. A major trade-off, of course, is the disruption in the sp^2-hybridized backbone of graphene upon basal plane covalent addition, which is often accompanied by a decrease in its charge carrier mobility. However, not all applications need a high charge carrier mobility and thus significant amount of research efforts have been directed towards the covalent functionalization of graphene. Apart from band structure modification, the general motivation behind the organic covalent functionalization of graphene has been to increase its solubility and for making composites of graphene with other materials.

Graphene benefits from the rich functionalization protocols developed for structurally related allotropes such as fullerenes and CNTs. Past experience with these materials indicates that the most attractive species for the reaction with sp^2 carbons of graphene are organic reactive intermediates such as free radicals, carbenes, nitrenes, and arynes. These species form covalent adducts with graphene through free radical addition, CH insertion or cycloaddition reactions.[110] Furthermore, graphene has also been used as a versatile Diels–Alder substrate that can function as either the diene or the dienophile depending on the choice of reaction conditions.[111] Apart from the organic molecular functionalization, a wide community of researchers have also pursued atomic covalent functionalization, which involves hydrogenation, oxygenation and halogenation reactions on the basal plane of graphene.[112] A number of recent review articles have summarized the different types of covalent chemistries carried out on graphene.[26–30] In the following sections we discuss the covalent modification of surface supported graphene with a focus on the fundamental aspects and applicability in band structure modification.

A. Covalent functionalization of graphene: fundamental aspects

Synthetic methods for the covalent modification of graphene have progressed substantially in the past few years. A number of these investigations however focused on the solution chemistry of graphene flakes where the covalent chemistry was usually preceded by the dispersion of graphite into graphene using typical intercalation methods.[113] The covalent modification of graphene supported by standard substrates such as SiC, SiO_2 *etc.* is relevant for applications in electronic devices since DFT calculations[114] predict that such modification would create a large band gap (~1–2 eV) in graphene – a long-standing goal in the field. Diazonium chemistry has been particularly popular for the covalent attachment of aryl groups to the basal plane of graphene, with the largest number of publications to date.[31,32,113,115–125] Raman spectroscopy, which has been an integral part of graphene research in general, serves even better in characterization of covalently grafted samples of graphene. The generation of sp^3-hybridized defects in graphene is associated with the appearance of a characteristic D-band at around 1350 cm^{-1} together with changes in G and 2D bands.[126]

The usefulness of aromatic diazonium salts for covalent modification of carbon surfaces has been known since the 1990s. Savéant and co-workers have documented the covalent modification of carbon surfaces by aryl radicals generated from the electrochemical reduction of diazonium salts.[43] The aryldiazonium salts however also react spontaneously with graphene. The reaction mechanism involves the transfer of an electron from graphene to the aryl diazonium cation, which converts the latter into an aryl radical with the loss of N_2. The aryl radical then attacks the sp^2-hybridized carbon of the graphene lattice thereby covalently attaching itself onto the basal plane. A side reaction in this process involves formation of oligomers *via* covalent bond formation between aryl radicals and already grafted aryl species on the graphene surface. The covalent bonding to the graphene carbon leads to a slight buckling of the graphene layer displacing the newly formed sp^3 carbon out of plane by ~0.7 Å. DFT calculations predict favorable attachment of the next aryl radical at the *para*-position. Assuming such (1,4) configuration of grafting, a maximum coverage of 11% is achievable theoretically for the attachment of phenyl radicals, largely attributed to steric hindrance.[127] Although the DFT calculations predict long-range ordering based on the thermodynamics of the reaction, the highly reactive nature of the radicals ensures that the reaction proceeds under kinetic control and thus long range ordering has been reported rarely.[124]

The spontaneous grafting of aryl radicals onto EG/SiC was first evaluated by Bekyarova *et al.* by immersing the EG substrates in acetonitrile solutions of 4-nitrophenyl diazonium tetrafluoroborate (4-NBD).[118] The presence of grafted nitrophenyl radicals was confirmed by the NO_2 symmetric and asymmetric stretching modes in FT-IR, as well as the XPS peaks of the N atoms of NO_2. Cyclic voltammetry (CV) measurements indicated good surface coverage of the grafted species and were further used to confirm the durability of such covalent modification by carrying out the reduction of the grafted aryl NO_2 groups to NH_2. The robustness of the material was demonstrated by heating the nitrophenyl modified EG at 200 °C in a vacuum followed by XPS characterization, which confirmed the presence of NO_2 groups after heating. In line with the expected degradation of charge carrier mobility upon introduction of defects in the graphene lattice, the covalent modification with nitrophenyl moieties resulted in doubling of the room temperature resistance of EG.

Since the spontaneous attachment of aryl radicals to graphene essentially depends on the electron transfer from graphene to the diazonium salt, the rate of the reaction is governed by various factors such as the density of states of the diazonium salt relative to the Fermi level of graphene, the number of graphene layers, defects, edge states and the electrostatic environment of graphene which is often dictated by the underlying substrate. Wang *et al.* studied the influence of substrate on the reactivity of monolayer graphene. CVD-G/Cu transferred to arbitrary substrates such as SiO_2, Al_2O_3, h-BN and an alkyl-terminated SiO_2 substrate were subjected to reaction with 4-NBD (Fig. 9). Raman spectroscopy was used to monitor the integrated intensity ratio of the G and D peaks, which is a measure of the concentration of covalent defect sites. Raman spectra of the graphene samples supported by different substrates before and after functionalization revealed that graphene supported by SiO_2 and Al_2O_3 is more reactive towards covalent functionalisation compared to that on h-BN or on alkyl-terminated SiO_2.

The difference in the reactivity arises due to the varying level of influence of each substrate on the local density of states of graphene. Since the rate limiting step is the electron transfer, the Fermi level of graphene determines the influence of each substrate on graphene reactivity. Analysis of 2D peak

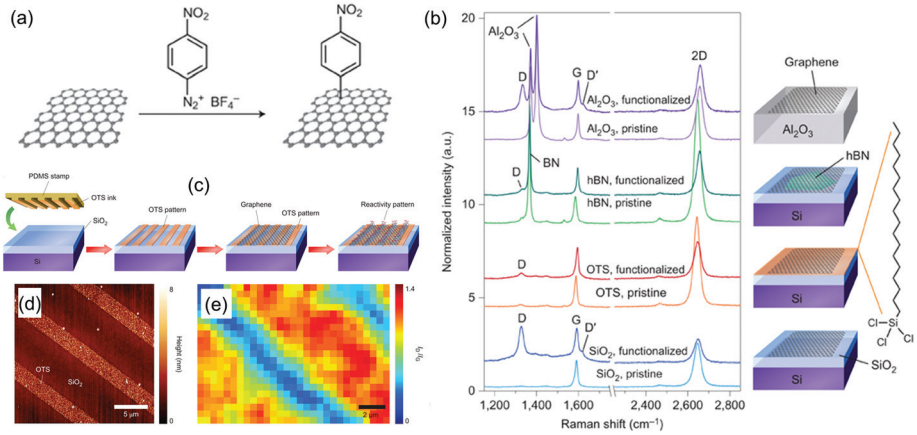

Fig. 9 Influence of the substrate on the diazonium chemistry of graphene. (a) Reaction scheme showing covalent functionalization of graphene using 4-NBD. (b) Representative Raman spectra of CVD-G transferred to different substrate materials before and after diazonium functionalization, normalized to the G peak height. These substrates are, from bottom to top, 300 nm thick SiO_2 on silicon, SiO_2 functionalized by an OTS self-assembled monolayer, single-crystal h-BN flakes deposited on SiO_2 and single-crystal α-Al_2O_3 (c-face sapphire). (c) Schematic illustration of reactive imprint lithography used to create patterned SiO_2 substrates. (d) AFM height image of the OTS functionalized SiO_2 substrate before graphene transfer. (e) Raman map of the I_D/I_G intensity ratio after diazonium functionalization. The narrow, mildly functionalized stripes (blue) correspond to the regions over the OTS pattern and the wide, strongly functionalized stripes (red) correspond to the regions over the SiO_2 gaps. Reproduced with permission.[117] (Copyright © 2012 Nature Publishing Group.)

positions of Raman spectra of pristine graphene samples revealed that the charge impurity puddles are stronger in graphene supported by SiO_2 and Al_2O_3 compared to the other two substrates. Such substrate induced electron–hole puddles are known to dope graphene thereby shifting its Fermi level. The authors also demonstrated micrometer level spatial control of reactivity using patterned substrates (Fig. 9c–e). Graphene transferred onto an SiO_2 substrate patterned with 2 μm wide lines of octadecyltrichlorosilane (OTS) was subjected to grafting by nitrophenyl radicals. A Raman spatial map of the covalently modified graphene revealed strong functionalization of graphene residing over the SiO_2 gaps compared to that resting on the alkyl chains of OTS.[117]

Besides the underlying substrate, the number of layers in graphene also influences the reactivity towards diazonium salts. The difference in reactivity between single layered and bilayer graphene flakes deposited on Si/SiO_2 was demonstrated by Koehler *et al.*[121] Time-dependent confocal Raman spectroscopy showed that the covalent attachment of nitrophenyl radicals occurs much faster on SLG with enhanced reactivity at the edges. Bilayer graphene on the other hand, was found to react rather sluggishly with the diazonium moieties. The authors suggested that the difference in reactivity between monolayer and bilayer graphene arises due to the reduced ability of the latter to accommodate a local sp^3 defect which in turn is related to its reduced flexibility compared to that of SLG.[121] The difference in the reactivity of monolayer and bilayer graphene is not specific to diazonium chemistry. Photocatalyzed decomposition of benzoyl peroxide in the presence of graphene also leads to the covalent attachment of phenyl radicals to the graphene surface and this reaction was reported to proceed ~14 times faster with SLG compared to bilayer graphene.[128] A more recent study involving direct imaging of the work function of mono- and multilayered graphene revealed that the graphene work function increases with the increasing number of layers which could be an additional factor that dictates its reactivity to electron transfer reactions.[129]

While graphene remains the focus of the research community in view of its technological importance, reports describing the covalent functionalization of HOPG also deserve a special mention here, as the same protocols can easily be adapted for graphene. A notable example is the patterning of HOPG using 4-carboxybenzenediazonium tetrafluoroborate (4-CBD). Kirkman *et al.* demonstrated the localized grafting of aryl groups onto the HOPG surface using diazonium chemistry under electrochemical control.[130] Micrometer level spatial control over the grafting process was achieved using scanning electrochemical cell microscopy (SECCM) wherein the exposure of 4-CBD to the HOPG substrate was precisely controlled using a narrow pipette. Using this approach, the authors could produce micrometer wide 4-CBD modified patches onto the HOPG surface in a controlled and reproducible fashion. While AFM topography measurements revealed the uniformity of covalent attachment under given experimental conditions (such as the applied potential and exposure time of diazonium meniscus to HOPG), Raman mapping of the modified substrate revealed the extent of covalent attachment to the HOPG surface. Although demonstrated on HOPG, this study outlines an elegant approach for the nano/microscale covalent modification of graphene as the diameter of the pipettes used in SECCM setup can be easily varied from a few hundred nanometers to tens of micrometers.[130] In a different study, Koehler *et al.* used lithography to pre-pattern HOPG using a photoresist mask, followed by exposure to diazonium reagents. KPFM and scanning electron microscopy (SEM)

revealed changes in the surface potential due to grafting by aryl groups with electron withdrawing ($-NO_2$) and donating ($-OCH_3$) functional groups.[131]

B. Covalent functionalization of graphene: band structure modification

The sp^3 centers produced after the covalent attachment of organic molecules to graphene act as defects and thus modify the effective conjugation length accessible to delocalized electrons. Such modification of the graphene lattice essentially represents patterning of the conjugation network and leads to changes in the band structure of graphene. For covalent modification of monolayer graphene, two different mechanisms are thought to be operative for band gap opening. (i) The generation of a large band gap (1–2 eV) in the immediate vicinity of sp^3 hybridized carbon centers. (ii) The opening of a small band gap (100 meV) in the pristine sp^2 lattice between two neighboring sp^3 clusters due to the quantum interference effect.[114,132] While the precise nanometer scale covalent patterning of graphene still remains elusive, random grafting of organic molecules has already been shown to modify the band structure of graphene.

Niyogi *et al.* used a combination of Raman and ARPES to characterize nitrophenyl-grafted graphene samples. Both exfoliated and EG/SiC were subjected to covalent functionalization by 4-NBD and subsequent spectroscopic analysis. For both graphene types, a prominent D-band appeared in the Raman spectra upon treatment with 4-NBD, indicating the generation of sp^3 defects. The band structure obtained from ARPES measurements after covalent modification revealed the opening of a band gap of ~0.4 eV.[31] Transport measurements carried out on nitrophenyl modified exfoliated graphene supported by the Si/SiO_2 substrate showed a decrease in the field effect mobility as well as device conductance which is consistent with the generation of defects in the graphene lattice. A band gap of 100 meV was accessible at 4 K using such covalent functionalization.[32]

Despite their extensive use for studying the non-covalent functionalization of graphene, scanning probe methods have seldom been employed to evaluate the extent of covalent grafting of organic molecules to graphene. Hossain *et al.*[120] employed UHV-STM for assessing the morphology of the graphene surface after covalent modification using 4-NBD (Fig. 10). Nitrophenyl modified EG/SiC substrates were annealed at 500 °C in a vacuum to remove any physisorbed contamination followed by STM imaging at room temperature. STM images revealed an inhomogeneous layer of irregularly shaped chain-like features, with visible patches of bare graphene surfaces (Fig. 10a). The peculiar surface morphology was attributed to the presence of aryl oligomers, which are formed due to the side reaction of nitrophenyl radicals in solution with those already grafted onto the graphene surface. The oligomer formation inhibits high density grafting since it

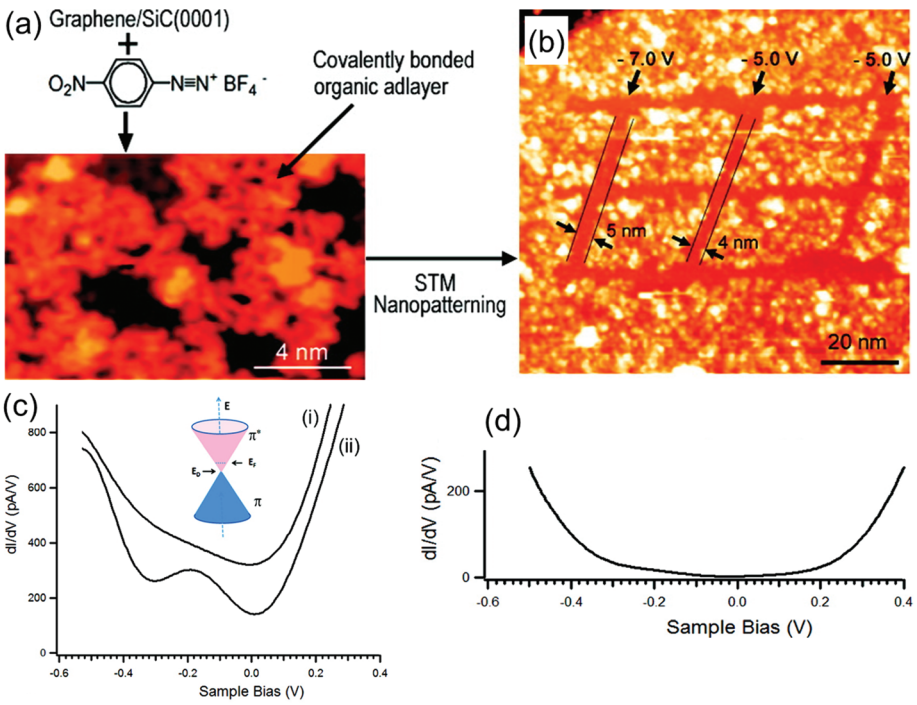

Fig. 10 Covalent modification of EG/SiC using 4-NBD. (a) STM image of the nitrophenyl modified graphene surface. (b) Bias-dependent nanopatterning of the aryl grafted graphene surface using STM. (c) d*I*/d*V* spectra obtained on the (i) aryl grafted regions of graphene and (ii) clean (unmodified) regions of graphene. (d) d*I*/d*V* spectrum showing the opening of a band gap in covalently modified graphene. Such STS spectra however represent a minority. Reproduced with permission.[120] (Copyright © 2010 American Chemical Society.)

physically blocks the surface. Scanning tunneling spectroscopy (STS) was employed to understand the electronic structure of the grafted substrates (Fig. 10c and d). STS spectra revealed that the electronic structure of graphene is not significantly perturbed within the regions where the physisorbed aryl oligomers reside. A minority of the STS spectra, which were assumed to be collected over the covalent attachment sites showed evidence of a band gap. STM based bias-dependent patterning allowed the fabrication of sub-5 nm lines within the covalently modified regions (Fig. 10b). These scratched regions are structurally akin to GNRs. Nevertheless, due to the low concentration of covalent binding sites at the edges of such structures, no quantum confinement effects were observed.[120]

Although DFT predicts a band gap as high as 2 eV in covalently functionalized graphene, there are practical aspects of covalent bonding onto the basal plane of graphene that impose limitations on the extent of electronic modification that can be achieved using this approach. Shih *et al.* established such limitations while investigating the electronic characteristics of nitrophenyl-functionalized exfoliated graphene flakes. Transport properties of nitrophenyl and bromophenyl-functionalized graphene devices were obtained at 14 K. A different extent of functionalization was achieved using the electrochemical reduction of diazonium cations in the presence of graphene devices and it was quantified from the I_D/I_G ratios obtained from Raman spectra. Based on the calculated average distance between the sp^3 centers, the authors concluded that only quantum interference effects should dominate the bandgap in such samples. Although the band gap of functionalized SLG was found to increase linearly with I_D/I_G ratios, it remained below 0.1 meV for SiO_2 supported graphene. Highly functionalized suspended graphene devices showed a bandgap of 1 meV, which is much lower than what is expected from quantum confinement effects (100 meV). The low band gap values obtained experimentally were attributed to the spatially inhomogeneous attachment of aryl groups (for suspended graphene) and the creation of mid-gap states that originate from charged impurities in the substrate (for G/SiO_2) during covalent functionalization.[132]

IV. Summary and outlook

The 'revolution' ignited by graphene in science and technology has intrigued chemists, physicists, biologists and engineers alike. After the initial surge of activity in the field that resulted in the publication of thousands of articles discussing the astonishing properties of the material, the focus has now shifted towards its use in different applications. Integrating graphene into real-life applications has been a daunting task though. The typical material and electronic properties of graphene have hindered its incorporation into useful devices and one of the ways forward is the modification of the material with organic molecules.

As discussed in-depth above, such functionalization has been achieved using covalent as well as non-covalent chemistries. The non-covalent approach appears to have evolved slightly more than the covalent approach, possibly in view of its simplicity. The adsorption of electron donating and withdrawing molecules onto the basal plane of graphene has been shown to induce n- and p-type doping of graphene, respectively. The results obtained so far constitute a good fundamental understanding of how the type and concentration of charge carriers in graphene can be manipulated by choice of organic adsorbates. Although the long-term stability of such supramolecular networks can be questioned, ultrathin organic membranes in the form of 2D COFs provide a robust alternative to supramolecular assemblies. The covalent chemistry on graphene is particularly attractive due to its predicted potential to open a band gap in graphene. While the experimental evidence obtained so far does point to the band gap opening upon the chemisorption of aryl groups, the magnitude of the gap is far from ideal. One of the reasons behind the inefficiency of the covalent approach in inducing a sizeable band gap in graphene is the lack of nanometer scale control over the process that leads to the random attachment of aryl groups.

An overview of the literature suggests that the 'surface-only' nature of SLG often acts as a double-edged sword. On the one hand it allows the easy modification of its electronic properties *via* simple adsorption of atoms and molecules, while on the other, it means that any adsorption (intentional or unintentional) on graphene is not inconsequential. This aspect becomes even more worrisome given the variable nature of doping offered by the substrates on which graphene resides. In view of these issues, the influence of substrates and unwanted contaminants always needs to be considered and de-convoluted from the targeted functionalization. Given that such contamination issues are addressed, the solution deposition approach, where organic molecules can be brought to the graphene surface under ambient conditions using a suitable solvent is promising due to its scalability.

Although plenty of work has already been done on organic functionalization of graphene, the control and tunability of covalent as well as non-covalent modification *vis-à-vis* the electronic properties of graphene remain virtually unexplored areas. Using the well-defined principles of supramolecular chemistry, it is possible to precisely tune the density of functional groups on the graphene surface, which in turn could potentially affect the level of doping. Furthermore, there is a pressing need to develop covalent chemistry protocols where the density and location of the grafted species can be precisely controlled. Such controlled covalent patterning of graphene will pave the way for opening of a band gap that is relevant for electronic applications. Scanning probe methods, especially STM is expected to play an increasingly important role in this context due to its ability to divulge the surface morphology at sub-molecular resolution, which will be useful to correlate the extent of functionalization with changes in graphene properties. Assuming that the 'dust has now settled' after

the initial quest for graphene functionalization, it is time to look at the issue from a more fundamental yet pragmatic point of view.

Acknowledgements

This work was supported by the Fund of Scientific Research–Flanders (FWO), KU Leuven (GOA 11/003), Belgian Federal Science Policy Office (IAP–7/05). This research has also received funding from the European Research Council under the European Union's Seventh Framework Programme (FP7/2007-2013)/ERC grant agreement no. 340324.

References

1 M. J. Allen, V. C. Tung and R. B. Kaner, *Chem. Rev.*, 2009, **110**, 132–145.
2 K. S. Novoselov, A. K. Geim, S. V. Morozov, D. Jiang, Y. Zhang, S. V. Dubonos, I. V. Grigorieva and A. A. Firsov, *Science*, 2004, **306**, 666–669.
3 A. K. Geim and K. S. Novoselov, *Nat. Mater.*, 2007, **6**, 183–191.
4 K. S. Novoselov, V. I. Falko, L. Colombo, P. R. Gellert, M. G. Schwab and K. Kim, *Nature*, 2012, **490**, 192–200.
5 S. V. Morozov, K. S. Novoselov, M. I. Katsnelson, F. Schedin, D. C. Elias, J. A. Jaszczak and A. K. Geim, *Phys. Rev. Lett.*, 2008, **100**, 016602.
6 C. Lee, X. Wei, J. W. Kysar and J. Hone, *Science*, 2008, **321**, 385–388.
7 F. Guinea, M. I. Katsnelson and A. K. Geim, *Nat. Phys.*, 2010, **6**, 30–33.
8 A. A. Balandin, *Nat. Mater.*, 2011, **10**, 569–581.
9 R. R. Nair, P. Blake, A. N. Grigorenko, K. S. Novoselov, T. J. Booth, T. Stauber, N. M. R. Peres and A. K. Geim, *Science*, 2008, **320**, 1308.
10 J. S. Bunch, S. S. Verbridge, J. S. Alden, A. M. van der Zande, J. M. Parpia, H. G. Craighead and P. L. McEuen, *Nano Lett.*, 2008, **8**, 2458–2462.
11 N. O. Weiss, H. Zhou, L. Liao, Y. Liu, S. Jiang, Y. Huang and X. Duan, *Adv. Mater.*, 2012, **24**, 5782–5825.
12 S. Stankovich, D. A. Dikin, G. H. B. Dommett, K. M. Kohlhaas, E. J. Zimney, E. A. Stach, R. D. Piner, S. T. Nguyen and R. S. Ruoff, *Nature*, 2006, **442**, 282–286.
13 Y. Shao, J. Wang, H. Wu, J. Liu, I. A. Aksay and Y. Lin, *Electroanalysis*, 2010, **22**, 1027–1036.
14 Q. He, S. Wu, Z. Yin and H. Zhang, *Chem. Sci.*, 2012, **3**, 1764–1772.
15 S. C. O'Hern, M. S. H. Boutilier, J.-C. Idrobo, Y. Song, J. Kong, T. Laoui, M. Atieh and R. Karnik, *Nano Lett.*, 2014, **14**, 1234–1241.
16 D. Cohen-Tanugi and J. C. Grossman, *Nano Lett.*, 2012, **12**, 3602–3608.
17 N. Zhang, Y. Zhang and Y.-J. Xu, *Nanoscale*, 2012, **4**, 5792–5813.
18 S. Pang, Y. Hernandez, X. Feng and K. Müllen, *Adv. Mater.*, 2011, **23**, 2779–2795.
19 Z. Liu, Q. Liu, Y. Huang, Y. Ma, S. Yin, X. Zhang, W. Sun and Y. Chen, *Adv. Mater.*, 2008, **20**, 3924–3930.
20 X. Wang, L. Zhi and K. Müllen, *Nano Lett.*, 2007, **8**, 323–327.
21 V. C. Tung, M. J. Allen, Y. Yang and R. B. Kaner, *Nat. Nanotechnol.*, 2009, **4**, 25–29.
22 Y. Lee, S. Bae, H. Jang, S. Jang, S.-E. Zhu, S. H. Sim, Y. I. Song, B. H. Hong and J.-H. Ahn, *Nano Lett.*, 2010, **10**, 490–493.
23 F. Schwierz, *Nat. Nanotechnol.*, 2010, **5**, 487–496.
24 Y. Hernandez, V. Nicolosi, M. Lotya, F. M. Blighe, Z. Sun, S. De, I. T. McGovern, B. Holland, M. Byrne, Y. K. Gun'Ko, J. J. Boland, P. Niraj, G. Duesberg, S. Krishnamurthy, R. Goodhue, J. Hutchison, V. Scardaci, A. C. Ferrari and J. N. Coleman, *Nat. Nanotechnol.*, 2008, **3**, 563–568.
25 A. Ciesielski and P. Samori, *Chem. Soc. Rev.*, 2014, **43**, 381–398.
26 V. Georgakilas, M. Otyepka, A. B. Bourlinos, V. Chandra, N. Kim, K. C. Kemp, P. Hobza, R. Zboril and K. S. Kim, *Chem. Rev.*, 2012, **112**, 6156–6214.
27 L. Yan, Y. B. Zheng, F. Zhao, S. Li, X. Gao, B. Xu, P. S. Weiss and Y. Zhao, *Chem. Soc. Rev.*, 2012, **41**, 97–114.
28 H. Liu, Y. Liu and D. Zhu, *J. Mater. Chem.*, 2011, **21**, 3335–3345.
29 K. P. Loh, Q. Bao, P. K. Ang and J. Yang, *J. Mater. Chem.*, 2010, **20**, 2277–2289.
30 Q. Tang, Z. Zhou and Z. Chen, *Nanoscale*, 2013, **5**, 4541–4583.
31 S. Niyogi, E. Bekyarova, M. E. Itkis, H. Zhang, K. Shepperd, J. Hicks, M. Sprinkle, C. Berger, C. N. Lau, W. A. deHeer, E. H. Conrad and R. C. Haddon, *Nano Lett.*, 2010, **10**, 4061–4066.
32 H. Zhang, E. Bekyarova, J.-W. Huang, Z. Zhao, W. Bao, F. Wang, R. C. Haddon and C. N. Lau, *Nano Lett.*, 2011, **11**, 4047–4051.
33 T. O. Wehling, K. S. Novoselov, S. V. Morozov, E. E. Vdovin, M. I. Katsnelson, A. K. Geim and A. I. Lichtenstein, *Nano Lett.*, 2007, **8**, 173–177.
34 X. Dong, D. Fu, W. Fang, Y. Shi, P. Chen and L.-J. Li, *Small*, 2009, **5**, 1422–1426.
35 W. Chen, S. Chen, D. C. Qi, X. Y. Gao and A. T. S. Wee, *J. Am. Chem. Soc.*, 2007, **129**, 10418–10422.
36 C. Coletti, C. Riedl, D. S. Lee, B. Krauss, L. Patthey, K. von Klitzing, J. H. Smet and U. Starke, *Phys. Rev. B: Condens. Matter*, 2010, **81**, 235401.
37 B. Li, A. V. Klekachev, M. Cantoro, C. Huyghebaert, A. Stesmans, I. Asselberghs, S. De Gendt and S. De Feyter, *Nanoscale*, 2013, **5**, 9640–9644.
38 J. M. P. Alaboson, Q. H. Wang, J. D. Emery, A. L. Lipson, M. J. Bedzyk, J. W. Elam, M. J. Pellin and M. C. Hersam, *ACS Nano*, 2011, **5**, 5223–5232.
39 F. Yavari, C. Kritzinger, C. Gaire, L. Song, H. Gulapalli, T. Borca-Tasciuc, P. M. Ajayan and N. Koratkar, *Small*, 2010, **6**, 2535–2538.

40 R. Balog, B. Jorgensen, L. Nilsson, M. Andersen, E. Rienks, M. Bianchi, M. Fanetti, E. Laegsgaard, A. Baraldi, S. Lizzit, Z. Sljivancanin, F. Besenbacher, B. Hammer, T. G. Pedersen, P. Hofmann and L. Hornekaer, *Nat. Mater.*, 2010, **9**, 315–319.
41 W. Zhang, C.-T. Lin, K.-K. Liu, T. Tite, C.-Y. Su, C.-H. Chang, Y.-H. Lee, C.-W. Chu, K.-H. Wei, J.-L. Kuo and L.-J. Li, *ACS Nano*, 2011, **5**, 7517–7524.
42 A. J. Samuels and J. D. Carey, *ACS Nano*, 2013, **7**, 2790–2799.
43 P. Allongue, M. Delamar, B. Desbat, O. Fagebaume, R. Hitmi, J. Pinson and J.-M. Savéant, *J. Am. Chem. Soc.*, 1997, **119**, 201–207.
44 J. A. A. W. Elemans, S. Lei and S. De Feyter, *Angew. Chem., Int. Ed.*, 2009, **48**, 7298–7332.
45 D. Tasis, N. Tagmatarchis, A. Bianco and M. Prato, *Chem. Rev.*, 2006, **106**, 1105–1136.
46 A. Hirsch, *Angew. Chem., Int. Ed.*, 2002, **41**, 1853–1859.
47 M. Prato, *J. Mater. Chem.*, 1997, **7**, 1097–1109.
48 F. Diederich and M. Gomez-Lopez, *Chem. Soc. Rev.*, 1999, **28**, 263–277.
49 L. S. Panchakarla, K. S. Subrahmanyam, S. K. Saha, A. Govindaraj, H. R. Krishnamurthy, U. V. Waghmare and C. N. R. Rao, *Adv. Mater.*, 2009, **21**, 4726–4730.
50 R. Lv, Q. Li, A. R. Botello-Méndez, T. Hayashi, B. Wang, A. Berkdemir, Q. Hao, A. L. Elías, R. Cruz-Silva, H. R. Gutiérrez, Y. A. Kim, H. Muramatsu, J. Zhu, M. Endo, H. Terrones, J.-C. Charlier, M. Pan and M. Terrones, *Sci. Rep.*, 2012, **2**, 586.
51 X. An, T. Simmons, R. Shah, C. Wolfe, K. M. Lewis, M. Washington, S. K. Nayak, S. Talapatra and S. Kar, *Nano Lett.*, 2010, **10**, 4295–4301.
52 J. M. MacLeod and F. Rosei, *Small*, 2014, **10**, 1038–1049.
53 G. M. Florio, T. L. Werblowsky, T. Müller, B. J. Berne and G. W. Flynn, *J. Phys. Chem. B*, 2005, **109**, 4520–4532.
54 S. De Feyter and F. C. De Schryver, *J. Phys. Chem. B*, 2005, **109**, 4290–4302.
55 S. Y. Zhou, G. H. Gweon, A. V. Fedorov, P. N. First, W. A. de Heer, D. H. Lee, F. Guinea, A. H. Castro Neto and A. Lanzara, *Nat. Mater.*, 2007, **6**, 770–775.
56 X. Wang, S. M. Tabakman and H. Dai, *J. Am. Chem. Soc.*, 2008, **130**, 8152–8153.
57 P. Lauffer, K. V. Emtsev, R. Graupner, T. Seyller and L. Ley, *Phys. Status Solidi (B)*, 2008, **245**, 2064–2067.
58 Q. H. Wang and M. C. Hersam, *Nat. Chem.*, 2009, **1**, 206–211.
59 H. Huang, S. Chen, X. Gao, W. Chen and A. T. S. Wee, *ACS Nano*, 2009, **3**, 3431–3436.
60 Q. H. Wang and M. C. Hersam, *Nano Lett.*, 2010, **11**, 589–593.
61 Y. Ogawa, T. Niu, S. L. Wong, M. Tsuji, A. T. S. Wee, W. Chen and H. Ago, *J. Phys. Chem. C*, 2013, **117**, 21849–21855.
62 A. Deshpande, C.-H. Sham, J. M. P. Alaboson, J. M. Mullin, G. C. Schatz and M. C. Hersam, *J. Am. Chem. Soc.*, 2012, **134**, 16759–16764.
63 B. Li, K. Tahara, J. Adisoejoso, W. Vanderlinden, K. S. Mali, S. De Gendt, Y. Tobe and S. De Feyter, *ACS Nano*, 2013, **7**, 10764–10772.
64 S. M. Kozlov, F. Viñes and A. Görling, *Adv. Mater.*, 2011, **23**, 2638–2643.
65 C.-H. Park, L. Yang, Y.-W. Son, M. L. Cohen and S. G. Louie, *Nat. Phys.*, 2008, **4**, 213–217.
66 W. Moritz, B. Wang, M. L. Bocquet, T. Brugger, T. Greber, J. Wintterlin and S. Günther, *Phys. Rev. Lett.*, 2010, **104**, 136102.
67 J. Wintterlin and M. L. Bocquet, *Surf. Sci.*, 2009, **603**, 1841–1852.
68 M. Roos, B. Uhl, D. Kunzel, H. E. Hoster, A. Gross and R. J. Behm, *Beilstein J. Nanotech.*, 2011, **2**, 365–373.
69 C. Meier, M. Roos, D. Künzel, A. Breitruck, H. E. Hoster, K. Landfester, A. Gross, R. J. Behm and U. Ziener, *J. Phys. Chem. C*, 2009, **114**, 1268–1277.
70 M. Roos, H. E. Hoster, A. Breitruck and R. J. Behm, *Phys. Chem. Chem. Phys.*, 2007, **9**, 5672–5679.
71 M. Roos, D. Künzel, B. Uhl, H.-H. Huang, O. Brandao Alves, H. E. Hoster, A. Gross and R. J. Behm, *J. Am. Chem. Soc.*, 2011, **133**, 9208–9211.
72 C. Mattevi, H. Kim and M. Chhowalla, *J. Mater. Chem.*, 2011, **21**, 3324–3334.
73 X. Sun, J. Zhang, X. Wang, C. Zhang, P. Hu, Y. Mu, X. Wan, Z. Guo and S. Lei, *Chem. Commun.*, 2013, **49**, 10317–10319.
74 P. Järvinen, S. K. Hämäläinen, K. Banerjee, P. Häkkinen, M. Ijäs, A. Harju and P. Liljeroth, *Nano Lett.*, 2013, **13**, 3199–3204.
75 H. G. Zhang, J. T. Sun, T. Low, L. Z. Zhang, Y. Pan, Q. Liu, J. H. Mao, H. T. Zhou, H. M. Guo, S. X. Du, F. Guinea and H. J. Gao, *Phys. Rev. B: Condens. Matter*, 2011, **84**, 245436.
76 J. Mao, H. Zhang, Y. Jiang, Y. Pan, M. Gao, W. Xiao and H. J. Gao, *J. Am. Chem. Soc.*, 2009, **131**, 14136–14137.
77 W. Dou, S. Huang, R. Q. Zhang and C. S. Lee, *J. Chem. Phys.*, 2011, **134**, 094705.
78 S. K. Hämäläinen, M. Stepanova, R. Drost, P. Liljeroth, J. Lahtinen and J. Sainio, *J. Phys. Chem. C*, 2012, **116**, 20433–20437.
79 Y.-L. Wang, J. Ren, C.-L. Song, Y.-P. Jiang, L.-L. Wang, K. He, X. Chen, J.-F. Jia, S. Meng, E. Kaxiras, Q.-K. Xue and X.-C. Ma, *Phys. Rev. B: Condens. Matter*, 2010, **82**, 245420.
80 K. S. Mali, J. Adisoejoso, E. Ghijsens, I. De Cat and S. De Feyter, *Acc. Chem. Res.*, 2012, **45**, 1309–1320.
81 H. J. Karmel, T. Chien, V. Demers-Carpentier, J. J. Garramone and M. C. Hersam, *J. Phys. Chem. Lett.*, 2013, **5**, 270–274.
82 Q. Zhou, Y. Li, Q. Li, Y. Wang, Y. Yang, Y. Fang and C. Wang, *Nanoscale*, 2014, **6**, 8387–8391.
83 P. C. M. Grim, S. De Feyter, A. Gesquière, P. Vanoppen, M. Rüker, S. Valiyaveettil, G. Moessner, K. Müllen and

F. C. De Schryver, *Angew. Chem., Int. Ed. Engl.*, 1997, **36**, 2601–2603.
84 S.-Y. Ding and W. Wang, *Chem. Soc. Rev.*, 2013, **42**, 548–568.
85 J. W. Colson, A. R. Woll, A. Mukherjee, M. P. Levendorf, E. L. Spitler, V. B. Shields, M. G. Spencer, J. Park and W. R. Dichtel, *Science*, 2011, **332**, 228–231.
86 L. Xu, X. Zhou, W. Q. Tian, T. Gao, Y. F. Zhang, S. Lei and Z. F. Liu, *Angew. Chem., Int. Ed.*, 2014, **53**, 9564–9568.
87 S. Ryu, L. Liu, S. Berciaud, Y.-J. Yu, H. Liu, P. Kim, G. W. Flynn and L. E. Brus, *Nano Lett.*, 2010, **10**, 4944–4951.
88 F. Schedin, A. K. Geim, S. V. Morozov, E. W. Hill, P. Blake, M. I. Katsnelson and K. S. Novoselov, *Nat. Mater.*, 2007, **6**, 652–655.
89 T. Ohta, A. Bostwick, T. Seyller, K. Horn and E. Rotenberg, *Science*, 2006, **313**, 951–954.
90 J. H. Chen, C. Jang, S. Adam, M. S. Fuhrer, E. D. Williams and M. Ishigami, *Nat. Phys.*, 2008, **4**, 377–381.
91 Y. Shi, X. Dong, P. Chen, J. Wang and L.-J. Li, *Phys. Rev. B: Condens. Matter*, 2009, **79**, 115402.
92 F. Varchon, R. Feng, J. Hass, X. Li, B. N. Nguyen, C. Naud, P. Mallet, J. Y. Veuillen, C. Berger, E. H. Conrad and L. Magaud, *Phys. Rev. Lett.*, 2007, **99**, 126805.
93 H. Pinto, R. Jones, J. P. Goss and P. R. Briddon, *J. Phys.: Condens. Matter*, 2009, **21**, 402001.
94 S. Barja, M. Garnica, J. J. Hinarejos, A. L. Vazquez de Parga, N. Martin and R. Miranda, *Chem. Commun.*, 2010, **46**, 8198–8200.
95 M. C. Prado, R. Nascimento, L. G. Moura, M. J. S. Matos, M. S. C. Mazzoni, L. G. Cancado, H. Chacham and B. R. A. Neves, *ACS Nano*, 2011, **5**, 394–398.
96 T. Zhang, Z. Cheng, Y. Wang, Z. Li, C. Wang, Y. Li and Y. Fang, *Nano Lett.*, 2010, **10**, 4738–4741.
97 X. Zhou, S. He, K. A. Brown, J. Mendez-Arroyo, F. Boey and C. A. Mirkin, *Nano Lett.*, 2013, **13**, 1616–1621.
98 B. Long, M. Manning, M. Burke, B. N. Szafranek, G. Visimberga, D. Thompson, J. C. Greer, I. M. Povey, J. MacHale, G. Lejosne, D. Neumaier and A. J. Quinn, *Adv. Funct. Mater.*, 2012, **22**, 717–725.
99 A. K. Singh, M. Ahmad, V. K. Singh, K. Shin, Y. Seo and J. Eom, *ACS Appl. Mater. Interfaces*, 2013, **5**, 5276–5281.
100 Y.-W. Son, M. L. Cohen and S. G. Louie, *Phys. Rev. Lett.*, 2006, **97**, 216803.
101 Y. Zhang, T.-T. Tang, C. Girit, Z. Hao, M. C. Martin, A. Zettl, M. F. Crommie, Y. R. Shen and F. Wang, *Nature*, 2009, **459**, 820–823.
102 Z. H. Ni, T. Yu, Y. H. Lu, Y. Y. Wang, Y. P. Feng and Z. X. Shen, *ACS Nano*, 2008, **2**, 2301–2305.
103 A. Narita, X. Feng, Y. Hernandez, S. A. Jensen, M. Bonn, H. Yang, I. A. Verzhbitskiy, C. Casiraghi, M. R. Hansen, A. H. R. Koch, G. Fytas, O. Ivasenko, B. Li, K. S. Mali, T. Balandina, S. Mahesh, S. De Feyter and K. Müllen, *Nat. Chem.*, 2014, **6**, 126–132.
104 R. Skomski, P. A. Dowben, M. Sky Driver and J. A. Kelber, *Mater. Horiz.*, 2014, **1**, 563–571.
105 S. M. George, *Chem. Rev.*, 2009, **110**, 111–131.
106 S. Kim, J. Nah, I. Jo, D. Shahrjerdi, L. Colombo, Z. Yao, E. Tutuc and S. K. Banerjee, *Appl. Phys. Lett.*, 2009, **94**, 062107.
107 S. Jandhyala, G. Mordi, B. Lee, G. Lee, C. Floresca, P.-R. Cha, J. Ahn, R. M. Wallace, Y. J. Chabal, M. J. Kim, L. Colombo, K. Cho and J. Kim, *ACS Nano*, 2012, **6**, 2722–2730.
108 D. B. Farmer, H.-Y. Chiu, Y.-M. Lin, K. A. Jenkins, F. Xia and P. Avouris, *Nano Lett.*, 2009, **9**, 4474–4478.
109 J. M. P. Alaboson, C.-H. Sham, S. Kewalramani, J. D. Emery, J. E. Johns, A. Deshpande, T. Chien, M. J. Bedzyk, J. W. Elam, M. J. Pellin and M. C. Hersam, *Nano Lett.*, 2013, **13**, 5763–5770.
110 J. Park and M. Yan, *Acc. Chem. Res.*, 2012, **46**, 181–189.
111 S. Sarkar, E. Bekyarova, S. Niyogi and R. C. Haddon, *J. Am. Chem. Soc.*, 2011, **133**, 3324–3327.
112 J. E. Johns and M. C. Hersam, *Acc. Chem. Res.*, 2012, **46**, 77–86.
113 J. M. Englert, C. Dotzer, G. Yang, M. Schmid, C. Papp, J. M. Gottfried, H.-P. Steinrück, E. Spiecker, F. Hauke and A. Hirsch, *Nat. Chem.*, 2011, **3**, 279–286.
114 D. W. Boukhvalov and M. I. Katsnelson, *Phys. Rev. B: Condens. Matter*, 2008, **78**, 085413.
115 Z. Jin, T. P. McNicholas, C.-J. Shih, Q. H. Wang, G. L. C. Paulus, A. J. Hilmer, S. Shimizu and M. S. Strano, *Chem. Mater.*, 2011, **23**, 3362–3370.
116 R. Sharma, J. H. Baik, C. J. Perera and M. S. Strano, *Nano Lett.*, 2010, **10**, 398–405.
117 Q. H. Wang, Z. Jin, K. K. Kim, A. J. Hilmer, G. L. C. Paulus, C.-J. Shih, M.-H. Ham, J. D. Sanchez-Yamagishi, K. Watanabe, T. Taniguchi, J. Kong, P. Jarillo-Herrero and M. S. Strano, *Nat. Chem.*, 2012, **4**, 724–732.
118 E. Bekyarova, M. E. Itkis, P. Ramesh, C. Berger, M. Sprinkle, W. A. de Heer and R. C. Haddon, *J. Am. Chem. Soc.*, 2009, **131**, 1336–1337.
119 A. Sinitskii, A. Dimiev, D. A. Corley, A. A. Fursina, D. V. Kosynkin and J. M. Tour, *ACS Nano*, 2010, **4**, 1949–1954.
120 M. Z. Hossain, M. A. Walsh and M. C. Hersam, *J. Am. Chem. Soc.*, 2010, **132**, 15399–15403.
121 F. M. Koehler, A. Jacobsen, K. Ensslin, C. Stampfer and W. J. Stark, *Small*, 2010, **6**, 1125–1130.
122 H. Lim, J. S. Lee, H.-J. Shin, H. S. Shin and H. C. Choi, *Langmuir*, 2010, **26**, 12278–12284.
123 D. B. Farmer, R. Golizadeh-Mojarad, V. Perebeinos, Y.-M. Lin, G. S. Tulevski, J. C. Tsang and P. Avouris, *Nano Lett.*, 2008, **9**, 388–392.
124 H. Zhu, P. Huang, L. Jing, T. Zuo, Y. Zhao and X. Gao, *J. Mater. Chem.*, 2012, **22**, 2063–2068.
125 F. Xiao-Yan, N. Ryo, Y. Li-Chang and T. Katsumi, *Nanotechnology*, 2010, **21**, 475208.
126 A. C. Ferrari and D. M. Basko, *Nat. Nanotechnol.*, 2013, **8**, 235–246.
127 D.-e. Jiang, B. G. Sumpter and S. Dai, *J. Phys. Chem. B*, 2006, **110**, 23628–23632.

128 H. Liu, S. Ryu, Z. Chen, M. L. Steigerwald, C. Nuckolls and L. E. Brus, *J. Am. Chem. Soc.*, 2009, **131**, 17099–17101.
129 C. Mathieu, N. Barrett, J. Rault, Y. Y. Mi, B. Zhang, W. A. de Heer, C. Berger, E. H. Conrad and O. Renault, *Phys. Rev. B: Condens. Matter*, 2011, **83**, 235436.
130 P. M. Kirkman, A. G. Güell, A. S. Cuharuc and P. R. Unwin, *J. Am. Chem. Soc.*, 2013, **136**, 36–39.
131 F. M. Koehler, N. A. Luechinger, D. Ziegler, E. K. Athanassiou, R. N. Grass, A. Rossi, C. Hierold, A. Stemmer and W. J. Stark, *Angew. Chem., Int. Ed.*, 2009, **48**, 224–227.
132 C.-J. Shih, Q. H. Wang, Z. Jin, G. L. C. Paulus, D. Blankschtein, P. Jarillo-Herrero and M. S. Strano, *Nano Lett.*, 2013, **13**, 809–817.